Lecturebook

ME 597: Mechanics of MEMS and NEMS

Purdue University
West Lafayette, IN

J.F. Rhoads (jfrhoads@purdue.edu)

Spring 2013
©2013

Contents

Chapter 1

Introduction and Scaling Laws

1.1 Introduction: A *Little* History

Unlike the history of the mechanics which govern them, the history of micro- and nanoelectromechanical systems (MEMS and NEMS), small-scale systems which integrate mechanical and electrical functionalities, is short and sweet. Most attribute the conception of such devices to the quirky, yet prescient, physicist Richard Feynman, who at a meeting of the American Physical Society in 1959 discussed the likely genesis of practical micro- and nanoscale technologies in his now seminal speech entitled, *There's Plenty of Room at the Bottom* [1, 2]. Little did Feynman know at the time, his ideas were not that far from fruition.

Six short years after Feynman's talk, amongst the sprawling hills of Western Pennsylvania at the Westinghouse Laboratories, Harvey Nathanson and his collaborators developed the first practical MEMS – a frequency-selective device that would later become known as the *resonant gate transistor* (see Fig. 1.1) [3, 4]. This tiny, bulk-fabricated device, measuring less than 1/10th of an inch in length with minimum feature sizes appreciably smaller, proved to be revolutionary. It opened engineers' minds to the possibility of small-scale electromechanical systems and moved Feynman's ideas from paper to practice.

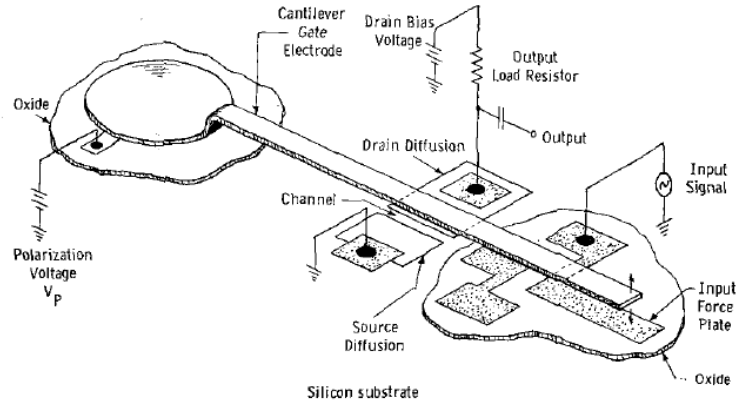

Figure 1.1: The resonant gate transistor – the original MEMS device. (From [4])

.

While the advances at Westinghouse demonstrated what was possible with a MEMS device, it only partially addressed what was practical. To truly penetrate industry, MEMS devices had to not only perform well in comparison to their more conventional, macroscale counterparts, but they had to be easily fabricated at low cost. This potentially damning hurdle was largely overcome on the back of Kurt Petersen's excellent 1982 review entitled, *Silicon as a Mechanical Material*, which not only characterized the many benefits of silicon-based structures, but more importantly highlighted the vast potential associated with electromechanical systems which are realized using modern integrated circuit (IC) fabrication techniques [5].

Today, MEMS and their nanoscale counterparts are seemingly everywhere. In the transportation sector, MEMS-based accelerometers are used for air-bag deployment and MEMS-based pressure sensors are used to monitor tire pressures. Likewise, in the consumer electronics sector, MEMS-based gyroscopes and accelerometers are used in gaming devices, such as the Nintendo Wii-mote,

and MEMS-based microphones and signal processing systems are used in cellular phones and PDAs. This is in addition to the multitude of MEMS-based technologies employed in biomedical applications (e.g., lab-on-chip sensors), defense applications (e.g., communications components and condition monitoring sensors), and even basic research (e.g., probe-based microscopy). A $72 billion dollar market today, MEMS and NEMS are surely here to stay.

1.2 This Lecturebook

The aforementioned explosion in MEMS/NEMS applications has come hand in hand with a very rapid expansion in MEMS/NEMS-related research. In 2011 alone more than 10,000 papers were published on the subject. As a result, it is nearly impossible to give a comprehensive and up-to-date review of the topic, even if the focus is narrowed to the subjects at hand.

In light of this, this lecturebook seeks to fill a niche. Specifically, it seeks to provide a high-level introduction to the modeling, analysis, and predictive design of MEMS and NEMS, which is accessible to advanced undergraduate students, graduate students, or practicing professionals with a background in engineering, physics, or applied mathematics. Given this breadth in target backgrounds, the lecturebook (and class) will undoubtedly cover material that you, the reader, already know. My apologies in advance! If you are interested in the subject, I also encourage you to look at some of the following references: [6–10].

By way of approach, this lecturebook focuses on both *first-principles* and *phenomenological* modeling; device-, component-, and system-level analyses; and, for the most part, classical physics. The basis for this is simple, to become proficient with MEMS and NEMS you need to be able to perform *back-of-the-envelope* calculations and develop an intuition about things which run counter to the experiences you have in the macroscale world. Because with MEMS and NEMS, multi-physics mechanisms dominate, noise becomes an important issue, and uncertainties become unavoidable.

In closing, please remember that *MEMS/NEMS modeling, analysis, and predictive design is a deceptive art founded upon sound science.* Likewise, *the modeling, analysis, and design techniques introduced herein are only as good as the experiment that validates them.*

1.3 Scaling Laws

Micro/nanoscale physics are non-intuitive. One needs to consistently benchmark and ask oneself: *What is really small?* This section seeks to introduce the tools necessary to answer this question. Additional details can be found in Reference [10].

Isometric Scaling

Let d be a unit of distance and l be a length benchmark. If $d = \alpha l$, where α is a known constant, then one would say distance scales with length l.

Using a similar procedure, let $A = wd$ be the area of a surface d units long and w units wide. If $d = \alpha l$ and $w = \beta l$, where α and β are known constants, then $A = wd = \alpha\beta l^2$ scales with l^2.

Likewise, let V be a volume d units long, w units wide, and h units tall. If $h = \delta l$, where δ is a known constant, then $V = wdh = \alpha\beta\delta l^3$ scales with l^3.

Key Result: Using the previous results one can compute the scaling of a surface-to-volume ratio:

$$\gamma = \frac{A}{V} = \frac{wd}{wdh} = \frac{1}{h} \propto \frac{1}{l} \tag{1.1}$$

From this result, it is clear that surface-to-volume ratio γ scales with l^{-1}. Accordingly, at small scales surface effects dominate volume effects. This means that surface forces, such as friction and fluid tensions, tend to dominate body forces and become markedly more important at the micro- and nanoscales than they are at the macroscale.

Key Result: The length scaling of mass m can be easily determined by noting that $m = \rho V$, where ρ is the mass density of the object in question. Since mass density is a material property, it is largely independent of length scale. Accordingly, m scales with l^3.

Key Result: Using similar logic, weight $W = mg$, where g is the local, scale-independent gravitational constant, can be shown to scale with l^3. Since weight is a volume effect, one can rightly conclude that the effects of gravity are largely negligible at small scales and thus can be omitted from most analyses without penalty.

Force Scaling

There are a wide array of transduction mechanisms employed in micro- and nanosystems for a wide variety of reasons. The following section brings some of these reasons to light by examining how force magnitudes scale with physical size.

Electrostatic Forces:

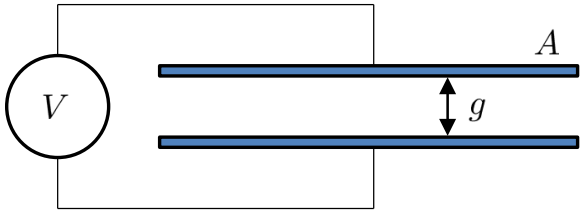

Figure 1.2

The attractive force between two charged, parallel plates (see Fig. 1.2) is given by

$$F = \frac{\varepsilon A V^2}{2g^2}, \tag{1.2}$$

where ε is the permittivity of the medium between the two plates, A is the overlapping plate area, g is the effective gap between the plates, and V represents the voltage between plates.

Assuming that V is constant with physical scale (a decent approximation for many applications), F scales with l^0. Thus, assuming that V is constant, electrostatic forces are scale independent. Given that body forces, such as weight, become smaller as length scales are reduced, electrostatic forces can, and frequently do, dominate.

In contrast, if g is *small* or V is *very large*, the system will be limited by electrical breakdown (whereupon the medium between the two plates becomes conductive). In this scenario, we are limited by the breakdown field $\mathcal{E}_{max}$. In a gaseous environment, $\mathcal{E}_{max}$ depends on both pressure and gas constants and $\mathcal{E}_{max} = V/g$ becomes a good approximation (i.e. the electric field becomes constant). Here, F scales like l^2. In this scenario, electrostatic forces do decrease with scale, but at a slower rate that body forces. Not surprisingly, the true scaling lays these two limiting scenarios.

Magnetic Forces: Consider two current-carrying conductors. The force between these conductors can be expressed as:

$$F = \frac{\mu_0 i^2 l}{2\pi g}, \tag{1.3}$$

where μ_0 is the permeability of the medium surrounding the conductors, l is the length of the conductors, i is the current passing through the conductors, and g represents the gap between the conductors. Assuming that the current is constant, F scales like l^0.

Though this scaling is encouraging, as before, the maximum value of i is practically constrained by the maximum current density that the conductors can handle J_{max}. Assuming $J_{max} = i/A$ and that the conductors have identical cross sections of area A, F suddenly scales like l^4. Therefore, the force scales *worse* than body forces. Could there be a redeeming benefit?

Thermal Forces: Consider the force produced by the heat-induced expansion of a simple rod:

$$F = EA\alpha\Delta T. \tag{1.4}$$

Here, E specifies the modulus of elasticity of the material, α represents the coefficient of thermal expansion and ΔT is the applied temperature change. Assuming that this temperature change is constant, F scales like l^2. Interestingly, one can also show that the time response of this system also scales with l^2, making thermal actuation an appealing design option at the micro- and nanoscales.

Piezoelectric Forces: Consider a d_{33} piezoelectric actuator (these will be discussed in much greater depth later in the text). The force produced by this system under an applied voltage is given by

$$F = \frac{EAd_{33}V}{t}, \tag{1.5}$$

where d_{33} is a piezoelectric constant and t is the thickness of the material. Assuming the applied voltage is constant, F scales with l.

As before, we can consider a breakdown-limited scenario as well. Assuming a constant electric field $\mathcal{E}_{max} = V/t$,

$$F = EAd_{33}\mathcal{E}_{max} \tag{1.6}$$

and F scales with l^2. Accordingly, piezoelectric forces may scale better than more classical alternatives. Why hasn't this transduction mechanism taken over the field?

Viscous Damping Forces: Viscous damping, as realized via a classical drag force model, is governed by

$$F = \frac{1}{2}C_d\rho A\dot{x}^n, \tag{1.7}$$

where C_d is a drag coefficient (a strong function of the system's geometry, but not size), A is a projected frontal area, and n is a speed constant specified to be 1 at *low* speeds and 2 at *moderate* to *high* speeds. Quick analysis of this model reveals that viscous forces scale with $l^2\dot{x}^n$, accordingly they often play a very important role at small scales.

Example 1.1

Given: The effective spring constant of a simple, rectangular cantilever with an applied point load at its free end is given by

$$k = \frac{3EI}{L^3},$$

where E represents the cantilever's modulus of elasticity (assumed to be scale-independent), I represents the system's cross-sectional moment of inertia, and L specifies the device's length.

Find: Determine the length scaling of the spring constant.

Example 1.2

Given: Consider the simple spring-mass system shown below. Under a given set of initial conditions (initial position and velocity), this system has a propensity to vibrate at a natural frequency given by

$$\omega_n = \sqrt{\frac{k}{m}},$$

where m represents the system's effective mass and k specifies the system's effective spring constant.

Find: Determine the length scaling of the system's natural frequency.

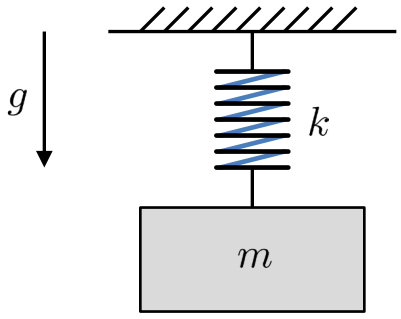

Example 1.3

Given: Consider the simple spring-mass system shown below. Under the influence of gravity, the mass displaces a static amount x_{st} from the undeformed position.

Find:
(a) Draw a Free Body Diagram of the system.
(b) Find an expression for the static offset x_{st} in terms of the given mass m, stiffness k, and gravitation constant g.
(c) Determine the length scaling of the system's static deflection.

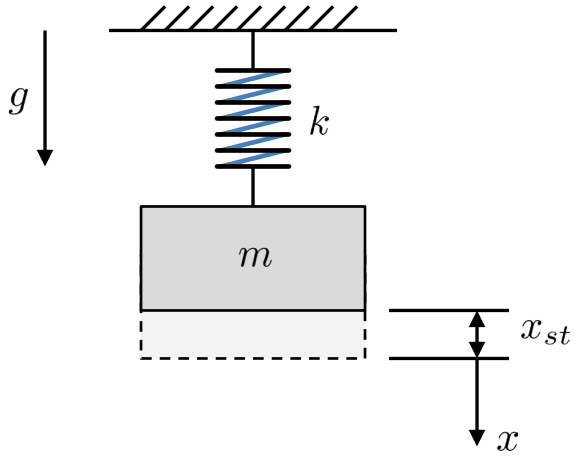

Example 1.4

Given: Consider the thermal displacement noise in a mechanical resonator:

$$x_{rms} = \sqrt{\frac{k_B T}{k}}.$$

Here k_B is Boltzman's constant, T is the temperature of the surrounding thermal bath, and k is the effective spring constant of the resonator.

Find: Determine the length scaling of the system's thermal displacement noise.

Example 1.5

Given: An engineer in your group has proposed replacing a cantilevered spring element with a rod or bar that undergoes axial extension. The spring constant of the proposed system is given by

$$k = \frac{EA}{L},$$

where E represents the system's modulus of elasticity (assumed to be scale-independent), A is the system's cross-sectional area, and L describes the length of the actuator.

Find: Determine how the spring constant of the proposed system scales with length. Compare or contrast the obtained scaling factor with that of the existing cantilevered system.

Example 1.6

Given: A MEMS start-up company has the goal of reducing the form factor of their new microactuator. As part of the re-design process, the company seeks to reduce all of their device dimensions by a factor of 4, and to determine whether their application would benefit more from piezoelectric or electrostatic actuation.

Find: Determine how the actuator displacement $x = F/k$ scales for each actuation scheme. Comment on each actuation scheme's relative utility. Assume that both actuators operate in the presence of a constant actuation voltage.

Chapter 2

Mechanical Modeling: Beams

2.1 Modeling Mechanical Elements

In a very generic sense, there are two distinct ways of modeling mechanical systems:

- **Distributed-Parameter Modeling** utilizes a first principles approach, founded upon Newton's Second Law and associated kinematics, to develop a spatially-distributed representation of the system.
- **Lumped-Parameter or Lumped-Mass Modeling** utilizes model reduction techniques, such as Galerkin methods or finite element methods, or a phenomenological approach to develop a spatially-independent representation of the system.

Successful MEMS/NEMS designers typically utilize distributed-parameter modeling and model reduction techniques to develop a tractable lumped-parameter model which is amenable to predictive design. Accordingly, this lecturebook will frequently adopt a similar technical approach.

2.2 Developing the Equation of Motion

Beams and beam-like structures permeate MEMS/NEMS research both as stand-alone devices and constituent elements. This chapter focuses on the application of thin beams as devices.

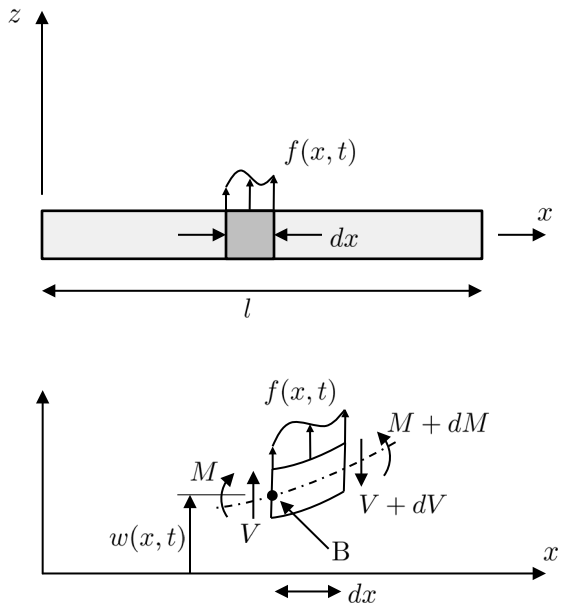

Figure 2.1

The equation of motion for a beam undergoing transverse deflection can be derived using an equilibrium approach (see, for example, [11]). Consider the differential element shown in Figure 2.1. Assuming small deflections and negligible rotation of the differential element, Newton's Second Law yields:

(2.1)

where ρ represents the beam's mass density, $A(x)$ is the beam's cross-sectional area, $M(x,t)$ defines the local bending moment, $V(x,t)$ defines the local shear force, and $f(x,t)$ is the applied transverse force per unit length.

Summing moments around point B while enforcing the aforementioned assumptions yields:

(2.2)

Mathematically, it proves helpful to re-write:

(2.3)

Substituting into the previous expressions yields:

(2.4)

(2.5)

Neglecting higher-order terms:

(2.6)

(2.7)

Substituting Equation (2.7) into Equation (2.6) yields

(2.8)

From Euler-Bernoulli beam theory:

(2.9)

where E represents the beam's modulus of elasticity and $I(x)$ is the cross-sectional area moment of inertia.

Substituting Equation (2.9) into Equation (2.8) yields:

$$\frac{\partial^2}{\partial x^2}\left[EI(x)\frac{\partial^2 w(x,t)}{\partial x^2}\right] + \rho A(x)\frac{\partial^2 w(x,t)}{\partial t^2} = f(x,t) \tag{2.10}$$

If the beam is uniform, that is $A(x) = A = \text{constant}$ and $I(x) = I = \text{constant}$, this becomes:

$$EI\frac{\partial^4 w(x,t)}{\partial x^4} + \rho A\frac{\partial^2 w(x,t)}{\partial t^2} = f(x,t) \tag{2.11}$$

Equations (2.10) and (2.11) can be analyzed using a variety of methods, providing initial and boundary conditions are known.

2.2.1 Common Initial Conditions

Initial displacement:

$$w(x,0) = w_0(x), \qquad 0 \le x \le l$$

Initial velocity:

$$\frac{\partial w(x,0)}{\partial t} = \dot{w}_0(x), \qquad 0 \le x \le l$$

2.2.2 Common Boundary Conditions

Free End:

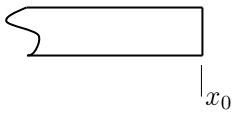

$$\frac{\partial}{\partial x}\left(EI\frac{\partial^2 w}{\partial x^2}\right)\bigg|_{(x_0,t)} = 0; \qquad \text{(Shear Force = 0)}$$

$$EI\frac{\partial^2 w(x_0,t)}{\partial x^2} = 0; \qquad \text{(Bending Moment = 0)}$$

Fixed End:

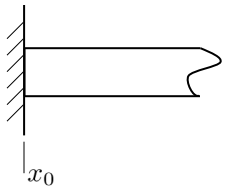

$$w(x_0,t) = 0; \qquad \text{(Displacement = 0)}$$

$$\frac{\partial w(x_0,t)}{\partial x} = 0; \qquad \text{(Slope = 0)}$$

Simply-Supported End:

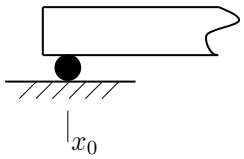

$$w(x_0, t) = 0; \qquad \text{(Displacement = 0)}$$

$$EI\frac{\partial^2 w(x_0, t)}{\partial x^2} = 0; \qquad \text{(Bending Moment = 0)}$$

2.3 Developing the Equation of Motion for Beams Carrying Axial Loads

While the previously-introduced beam model suffices for many geometric configurations, systems with fixed-fixed boundary conditions often can be better modeled if some axial effects are included. In MEMS/NEMS these effects are particularly important due to the prevalence of fabrication-induced axial stresses. Fortunately, the procedure required to derive the equation of motion for such systems largely mirrors that which was utilized before [11].

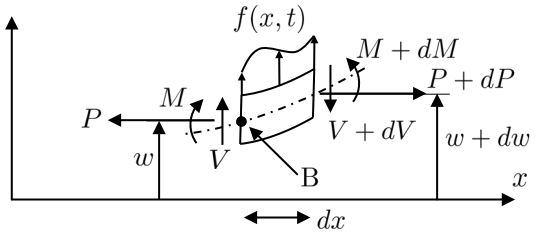

Figure 2.2

Consider the differential element shown in Figure 2.2. Assuming small deflections and negligible rotation of the differential element, Newton's Second Law yields:

(2.12)

where ρ represents the beam's mass density, $A(x)$ is the beam's cross-sectional area, $M(x,t)$ defines the local bending moment, $V(x,t)$ defines the local shear force, $f(x,t)$ is the external force per unit length applied transversely, and $P(x,t)$ is the external axial load.

Summing moments around point B while enforcing the aforementioned assumptions yields:

(2.13)

As before, let:

(2.14)

Substituting these expressions into the previous expressions yields:

(2.15)

(2.16)

Neglecting higher-order terms:

(2.17)

(2.18)

Substituting the previous result renders:

(2.19)

From Euler-Bernoulli beam theory:

(2.20)

where E represents the beam's modulus of elasticity and $I(x)$ is the cross-sectional area moment of inertia.

Substituting as appropriate yields:

$$\frac{\partial^2}{\partial x^2}\left[EI(x)\frac{\partial^2 w(x,t)}{\partial x^2}\right] + \rho A(x)\frac{\partial^2 w(x,t)}{\partial t^2} - \frac{\partial}{\partial x}\left[P(x,t)\frac{\partial w}{\partial x}\right] = f(x,t) \tag{2.21}$$

If the beam is uniform, that is $A(x) = A =$ constant and $I(x) = I =$ constant, and the axial load is constant, that is $P(x,t) = P =$ constant this becomes:

$$EI\frac{\partial^4 w(x,t)}{\partial x^4} + \rho A\frac{\partial^2 w(x,t)}{\partial t^2} - P\frac{\partial^2 w(x,t)}{\partial x^2} = f(x,t) \tag{2.22}$$

As before, Equations (2.21) and (2.22) can be analyzed using a variety of methods, providing initial and boundary conditions are known.

2.4 Other Beam Modeling Considerations

Though the previously developed equations of motion provide a sound foundation for analysis, they frequently must be modified to account for the exact system of interest. Two common modifications are described here.

2.4.1 Wide Beams

When the width of a beam exceeds roughly five times its thickness, it is often considered to be an elastic plates undergoing bending in one dimension [9]. In this *wide beam* scenario it is wise to modify the modulus of elasticity used with the model such that

$$E' = \frac{E}{1-\nu^2} \tag{2.23}$$

where E is the conventional modulus of elasticity and ν is Poisson's Ratio.

2.4.2 Laminated Composite Beams

Given the prevalence of bottom-up fabrication, it is not uncommon to see layered composite microstructures. In these scenarios an alternate flexural rigidity $(EI)'$ and effective mass $(\rho A)'$ are utilized:

$$(EI)' = \sum_{k=1}^{n} E_k I_k \tag{2.24}$$

$$(\rho A)' = \sum_{k=1}^{n} \rho_k A_k \tag{2.25}$$

where E_k, A_k, and ρ_k are the modulus of elasticity, cross-section area, and mass density of the kth layer, I_k is the area moment of inertia of the kth layer about the neutral axis of the beam, and n is the total number of layers in the composite. Note that the computation of I_k requires knowledge of the location of the neutral axis with respect to some reference surface. This distance z_{na} is given by

$$z_{na} = \frac{\sum_{k=1}^{n} E_k A_k z_k}{\sum_{k=1}^{n} E_k A_k}, \tag{2.26}$$

where z_k is the distance from a reference surface to the center of the kth layer.

For additional information on composite structures, the interested reader should consider Reference [12].

Example 2.1

Given: Consider a cantilevered beam of length L with a rectangular cross-section ($I, A =$ constant) and an applied transverse distributed load (force per unit length) of constant magnitude P.

Find:
(a) Determine the tip deflection of the beam $w(L)$.
(b) Determine the effective *stiffness* parameter which relates the net force to the tip deflection found in part (a).

Example 2.2

Given: Consider a cantilevered beam of length L with a rectangular cross-section ($I, A =$ constant) and an applied transverse point load on the free end of constant magnitude F.

Find:
(a) Determine the tip deflection of the beam $w(L)$.
(b) Determine the effective *stiffness* parameter which relates the net force to the tip deflection found in part (a).

Chapter 3

Mechanical Modeling: Plates and Membranes

3.1 Developing the Equation of Motion for Thin Plates

In a very generic sense, plates are two-dimensional extensions of beams. Because of this, equilibrium methods similar to those utilized in the previous module for beams can be used to develop a representative equation of motion [11]. Before proceeding, it is helpful to make a few assumptions:

- The plate thickness h is small in comparison to the the plate's length and width.
- The neutral axis of the plate is centrally located and does not undergo in-plane deformation.
- The transverse deflection $w(x, y, t)$ defined at the middle surface (downward positive) is small compared to h.
- Transverse shear deformation is negligible.
- Rotational inertia is negligible.

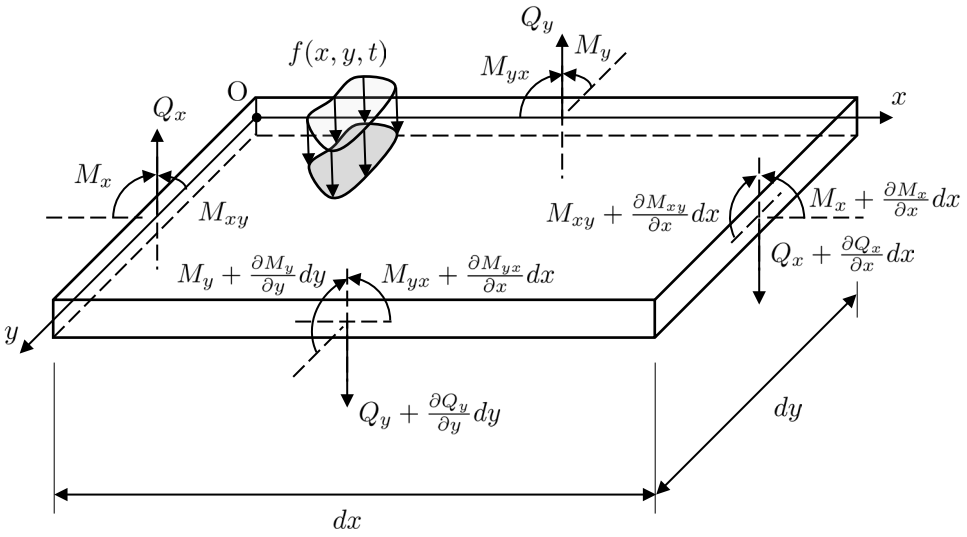

Figure 3.1

Consider the differential element shown in Figure 3.1. Assuming small deflections and negligible rotation of the differential element, Newton's Second Law yields:

(3.1)

where Q_x and Q_y are the force resultants per unit length and ρ is the mass density of the plate's material.

Simplifying this expression yields:

(3.2)

Summing moments about the x-axis renders:

(3.3)

where M_x and M_y, M_{xy} and M_{yx} are moment resultants per unit length.

Ignoring higher-order terms:

(3.4)

Likewise, summing moments about the y-axis yields:

$$Q_x = \frac{\partial M_x}{\partial x} + \frac{\partial M_{xy}}{\partial y} \tag{3.5}$$

Recall that stress is a tensor quantity with elements:

$$\boldsymbol{\sigma} = \begin{pmatrix} \sigma_{xx} & \sigma_{xy} & \sigma_{xz} \\ \sigma_{yx} & \sigma_{yy} & \sigma_{yz} \\ \sigma_{zx} & \sigma_{zy} & \sigma_{zz} \end{pmatrix}. \tag{3.6}$$

Because the plate has comparatively-low thickness, the normal stress in the z-direction can be neglected:

$$\sigma_{zz} = 0. \tag{3.7}$$

Likewise, because only bending deformations are considered here, there are no induced in-plane resultant forces:

$$\int_{-h/2}^{h/2} \sigma_{xx} dz = 0, \tag{3.8}$$

$$\int_{-h/2}^{h/2} \sigma_{yy} dz = 0. \tag{3.9}$$

Likewise,

$$M_x = \int_{-h/2}^{h/2} \sigma_{xx} z dz \tag{3.10}$$

$$M_y = \int_{-h/2}^{h/2} \sigma_{yy} z dz \tag{3.11}$$

$$M_{xy} = M_{yx} = \int_{-h/2}^{h/2} \sigma_{xy} z dz \qquad (\sigma_{xy} = \sigma_{yx}) \tag{3.12}$$

$$Q_x = \int_{-h/2}^{h/2} \sigma_{xz} dz \tag{3.13}$$

$$Q_y = \int_{-h/2}^{h/2} \sigma_{yz} dz \tag{3.14}$$

To derive the equation of motion, strain-displacement relationships are also required. To acquire these consider the following elements:

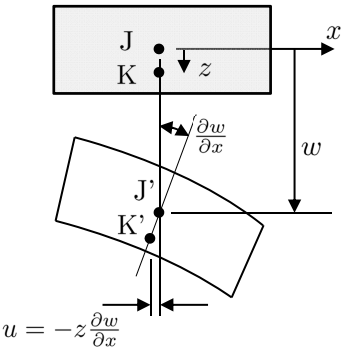

Analysis of the element reveals

(3.15)

Similarly,

(3.16)

From elasticity, it is known that

(3.17)

Substituting yields:

$$\varepsilon_{xx} = -z\frac{\partial^2 w}{\partial x^2} \tag{3.18}$$

$$\varepsilon_{yy} = -z\frac{\partial^2 w}{\partial y^2} \tag{3.19}$$

$$\varepsilon_{xy} = -2z\frac{\partial^2 w}{\partial x \partial y} \tag{3.20}$$

Finally, assuming plane stress:

(3.21)

(3.22)

(3.23)

where E represents the plate's modulus of elasticity, G specifies the plate's shear modulus, and ν is Poisson's ratio.

Substituting yields:

$$M_x = -D\left(\frac{\partial^2 w}{\partial x^2} + \nu\frac{\partial^2 w}{\partial y^2}\right) \tag{3.24}$$

$$M_y = -D\left(\frac{\partial^2 w}{\partial y^2} + \nu\frac{\partial^2 w}{\partial x^2}\right) \tag{3.25}$$

$$M_{xy} = M_{yx} = -(1-\nu)D\frac{\partial^2 w}{\partial x \partial y} \tag{3.26}$$

where the the flexural rigidity D is given by:

$$D = \frac{Eh^3}{12(1-\nu^2)} \tag{3.27}$$

Likewise,

$$Q_x = -D\frac{\partial}{\partial x}\left(\frac{\partial^2 w}{\partial x^2} + \frac{\partial^2 w}{\partial y^2}\right) \tag{3.28}$$

$$Q_y = -D\frac{\partial}{\partial y}\left(\frac{\partial^2 w}{\partial x^2} + \frac{\partial^2 w}{\partial y^2}\right) \tag{3.29}$$

Substituting (yet again) yields:

$$D\left(\frac{\partial^4 w(x,y,t)}{\partial x^4} + 2\frac{\partial^4 w(x,y,t)}{\partial x^2 \partial y^2} + \frac{\partial^4 w(x,y,t)}{\partial y^4}\right) + \rho h\frac{\partial^2 w(x,y,t)}{\partial t^2} = f(x,y,t) \tag{3.30}$$

This is commonly written as:

$$D\nabla^4 w(x,y,t) + \rho h\frac{\partial^2 w(x,y,t)}{\partial t^2} = f(x,y,t), \tag{3.31}$$

where ∇^4 is a biharmonic operator.

If the plate is under an axial tension of magnitude T, this equation of motion becomes:

$$D\nabla^4 w(x,y,t) + \rho h\frac{\partial^2 w(x,y,t)}{\partial t^2} - T\nabla^2 w(x,y,t) = f(x,y,t). \tag{3.32}$$

As before, these equations of motion can be solved using a wide variety of methods provided that one has both boundary and initial conditions. In many instances this can be quite a mathematical challenge!

3.1.1 Common Initial Conditions

Initial displacement:

$$w(x, y, 0) = w_0(x, y), \tag{3.33}$$

Initial velocity:

$$\frac{\partial w(x, y, 0)}{\partial t} = \dot{w}_0(x, y) \tag{3.34}$$

3.1.2 Common Boundary Conditions

To fully constrain a plate in space, two boundary conditions are required on each edge. Since this leads to a series of eight boundary conditions for a rectangular plate geometry, it proves expedient to express the boundary conditions in terms of the local coordinates n and s which are normal and transverse to a given edge, respectively.

Free Edge:

$V_n = 0;$ (Shear Force = 0)

$M_n = 0;$ (Bending Moment = 0)

Fixed Edge:

$w = 0;$ (Displacement = 0)

$\frac{\partial w}{\partial n} = 0;$ (Slope = 0)

Simply-Supported Edge:

$w = 0;$ (Displacement = 0)

$M_n = 0;$ (Bending Moment = 0)

Note that the exact form for V_n and M_n can be derived using the the expressions developed in the previous subsection.

Key Result: Consider the plate of length a and width b shown below.

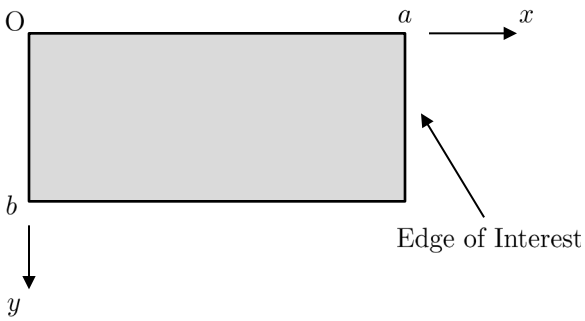

If the edge of interest is *free*, using the above result yields:

$$V_x = Q_x + \frac{\partial M_{xy}}{\partial y} = -D\left[\frac{\partial^3 w}{\partial x^3} + (2-\nu)\frac{\partial^3 w}{\partial x \partial y^2}\right]\Bigg|_{(a,y,t)} = 0, \tag{3.35}$$

$$M_x = -D\left(\frac{\partial^2 w}{\partial x^2} + \nu\frac{\partial^2 w}{\partial y^2}\right)\Bigg|_{(a,y,t)} = 0. \tag{3.36}$$

If the edge of interest is *fixed*, using the above result yields:

$$w(a,y,t) = 0, \tag{3.37}$$

$$\frac{\partial w}{\partial x}\Bigg|_{(a,y,t)} = 0. \tag{3.38}$$

If the edge of interest is *simply-supported*, using the above result yields:

$$w(a,y,t) = 0, \tag{3.39}$$

$$M_x = -D\left(\frac{\partial^2 w}{\partial x^2} + \nu\frac{\partial^2 w}{\partial y^2}\right)\Bigg|_{(a,y,t)} = \frac{\partial^2 w}{\partial x^2}\Bigg|_{(a,y,t)} = 0. \tag{3.40}$$

3.1.3 Round Plates

Note that the previously developed results can be extended to circular plates. This extension renders an equation of motion given by:

$$D\nabla^4 w(r,\theta,t) + \rho h \frac{\partial^2 w(r,\theta,t)}{\partial t^2} = f(r,\theta,t), \tag{3.41}$$

where r and θ represent the polar description of motion.

Here, however, one must be very careful evaluating the biharmonic operator, as the equation of motion written explicitly becomes

$$\begin{aligned} D\left(\frac{\partial^4 w}{\partial r^4} + \frac{2}{r}\frac{\partial^3 w}{\partial r^3} - \frac{1}{r^2}\frac{\partial^2 w}{\partial r^2} + \frac{1}{r^3}\frac{\partial w}{\partial r} + \frac{2}{r^2}\frac{\partial^4 w}{\partial r^2 \partial \theta^2} - \frac{2}{r^3}\frac{\partial^3 w}{\partial r \partial \theta^2} + \frac{4}{r^4}\frac{\partial^2 w}{\partial \theta^2} + \frac{1}{r^4}\frac{\partial^4 w}{\partial \theta^4}\right) \\ + \rho h \frac{\partial^2 w}{\partial t^2} = f(r,\theta,t) \end{aligned} \tag{3.42}$$

3.2 Modeling the Transverse Deflection of a Membrane

Membranes can be thought of as plates which have no bending stiffness. In these systems an applied load is used to keep the surface *taut*. Though improved model fidelity can be achieved with plate-like models, in some instances (e.g., very large area to thickness ratios) a simplified membrane model may suffice.

Consider the differential element shown below.

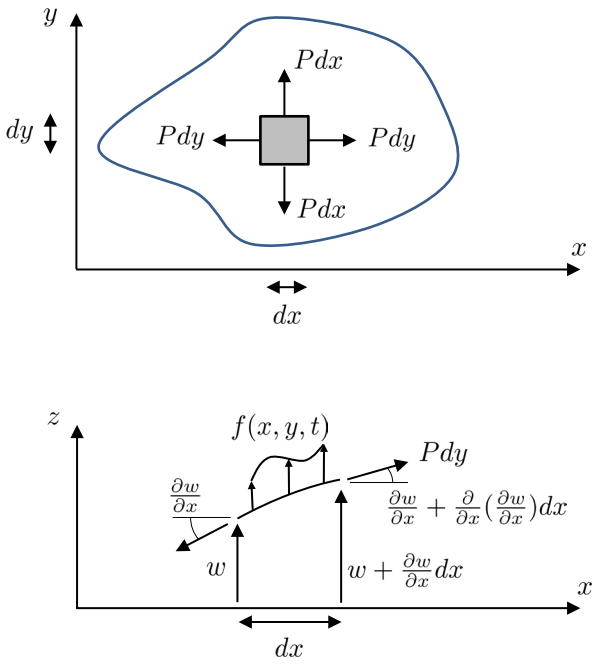

Applying Newton's Second Law:

(3.43)

where ρ is the mass of the membrane per unit area and P is a uniform applied force. Note that in the absence of the applied load P this equation becomes the 2D wave equation.

For circular membranes this becomes:

$$P\nabla^2 w(r,\theta,t) + f(r,\theta,t) = \rho\frac{\partial^2 w(r,\theta,t)}{\partial t^2}, \tag{3.44}$$

where

$$\nabla^2 = \frac{\partial^2}{\partial r^2} + \frac{1}{r}\frac{\partial}{\partial r} + \frac{1}{r^2}\frac{\partial^2}{\partial \theta^2}. \tag{3.45}$$

3.3 A Final Note on Mechanical Modeling

Thus far, this lecturebook has emphasized the modeling of devices where the plate, membrane, or beam is the integral mechanical component of the device. In practice this is often true, but these structures can also be used solely as support structures. In these scenarios it proces helpful to use tabulated stiffness values or finite element approaches.

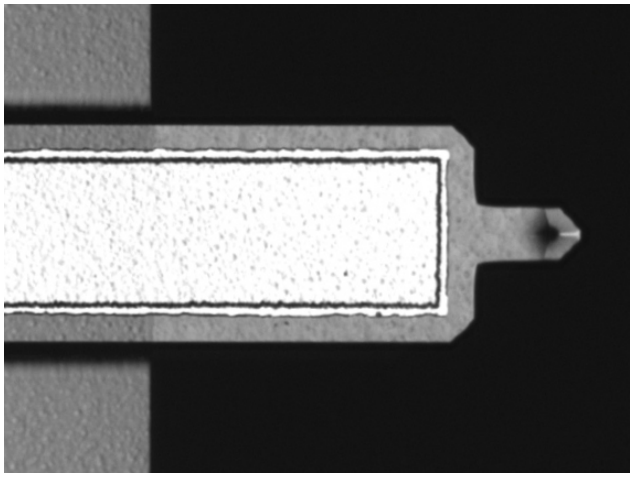

Figure 3.2: A piezoelectrically-actuated VEECO utilized for scanning probe microscopy and sensing applications [13]. In this system, the beam is the predominant mechanical component.

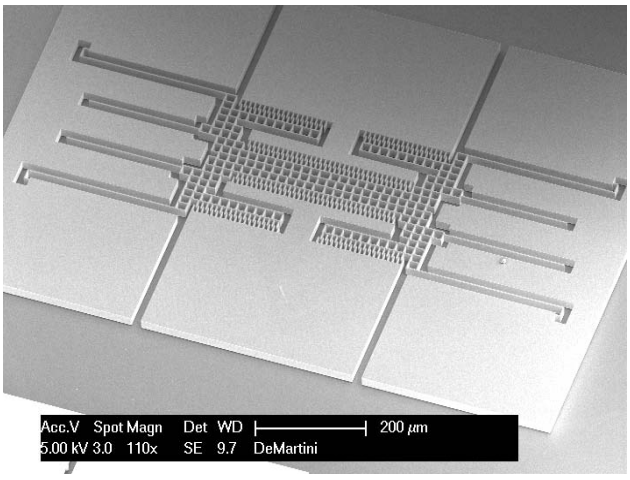

Figure 3.3: An electrostatically-actuated resonant mass sensor. In this system, beams are used for both support and sensing elements.

Chapter 4

Mechanical Modeling: Single-Degree-of-Freedom Resonators

4.1 Mechanical Resonators: A Review of Lumped-Mass Modeling and Analysis

Thus far, the lectures have focused on the modeling of beams, plates, and membranes and the analysis of static and quasistatic behaviors. The focus will now shift to the dynamic behavior of micro/nanoresonator, which are commonly found in radio-frequency (RF) signal processing and chemical/biological sensing systems amongst many others.

4.1.1 The Equation of Motion for a Single-Degree-of-Freedom Resonator

Lumped-mass resonators can be modeled as single-degree-of-freedom (SDOF) mass-spring-dashpot systems excited by an applied load.

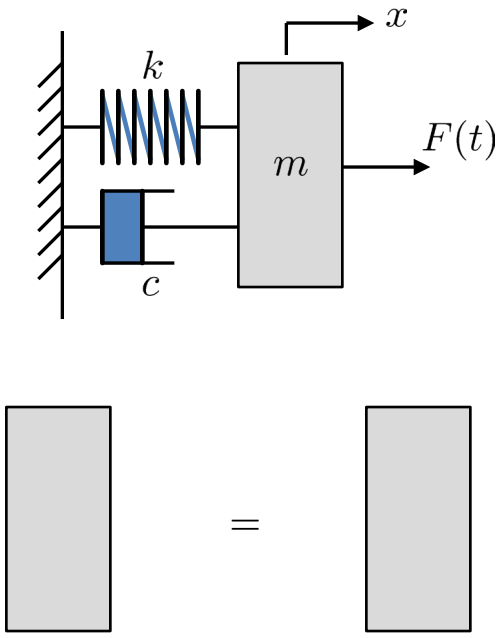

Applying Newton's Second Law:

(4.1)

where m, c and k prescribe the system's effective mass, damping, and stiffness respectively, x defines the resonator's displacement from equilibrium, and $F(t)$ is applied force.

Commonly, this equation is rescaled for the sake of interpretation as

(4.2)

(4.3)

or

(4.4)

where

(4.5)

is the natural frequency at which the system *likes* to vibrate at,

(4.6)

is the damping ratio associated with the system, and Q is the quality factor associated with the system.

Key Result: An appreciable amount of information about the system and its response can be recovered solely by examining ζ and Q. For example,

- If $0 \leq \zeta < 1$, the system is said to be *underdamped*. This condition corresponds to an oscillatory free response.
- If $\zeta = 1$, the system is said to be *critically damped*. This condition corresponds to the onset of a non-oscillatory free response.
- If $\zeta > 1$, the system is said to be *overdamped*. This condition corresponds to a non-oscillatory free response.

Likewise, the quality factor Q, defined according to

$$Q = \frac{1}{2\zeta} \tag{4.7}$$

holds distinct physical meaning. Namely, it is proportional (2π) to the ratio between the maximum amount of energy stored in a system and the amount of energy dissipated per cycle of motion. If Q is sufficiently large, its value roughly corresponds to the number of oscillations over which the resonator's energy falls to $e^{-2\pi}$ of its original value.

4.1.2 The Response of a Single-Degree-of-Freedom Resonator

The solution to the equation of motion given by Equation (4.3) has two distinct parts:

$$x(t) = x_h(t) + x_p(t). \tag{4.8}$$

Here, $x_h(t)$ describes the homogenous solution of the differential equation, which governs the free vibration of the system, and $x_p(t)$ describes the particular solution of the differential equation, which governs the forced vibration of the system. Physically speaking, if $\zeta \neq 0$, $x_p(t)$ will describe the system's steady-state behavior, and both $x_h(t)$ and $x_p(t)$ will contribute to transient behaviors.

The homogeneous solution $x_h(t)$ can be recovered by setting the excitation $F(t) = 0$ and solving the resulting differential equation:

$$\ddot{x} + 2\zeta\omega_n\dot{x} + \omega_n^2 x = 0. \tag{4.9}$$

Assume

(4.10)

Substitution reveals

(4.11)

The roots of the characteristic equation are thus

(4.12)

Accordingly, the homogeneous solution is given by:

(4.13)

where c_1 and c_2 are constants recovered through the application of initial conditions:

$$x(t=0) = x_0; \qquad \dot{x}(t=0) = \dot{x}_0. \tag{4.14}$$

Note that as long as $\zeta > 0$, $x_h(t) \to 0$ as $t \to \infty$.

The particular solution to a harmonic excitation of the form $F(t) = F \sin \omega t$ can be recovered by solving the following differential equation highlighted below using the Method of Assumed Solutions. While responses to non-harmonic inputs can be easily recovered through the use of convolution or Laplace methods, they are neglected here for the sake of brevity.

$$\ddot{x} + 2\zeta\omega_n\dot{x} + \omega_n^2 x = \frac{F}{m}\sin\omega t \tag{4.15}$$

Assume

(4.16)

Substituting this result and solving for X and ϕ yields

(4.17)

(4.18)

where the frequency ratio r is defined to be

(4.19)

Plotting X and ϕ as a function of the frequency ratio reveals the resonant nature of the system's frequency response.

Note that when $\omega = \omega_n$ ($r = 1$) the system resonates. However, this is not necessarily the excitation condition that leads to maximum displacement, due to the effects of damping!

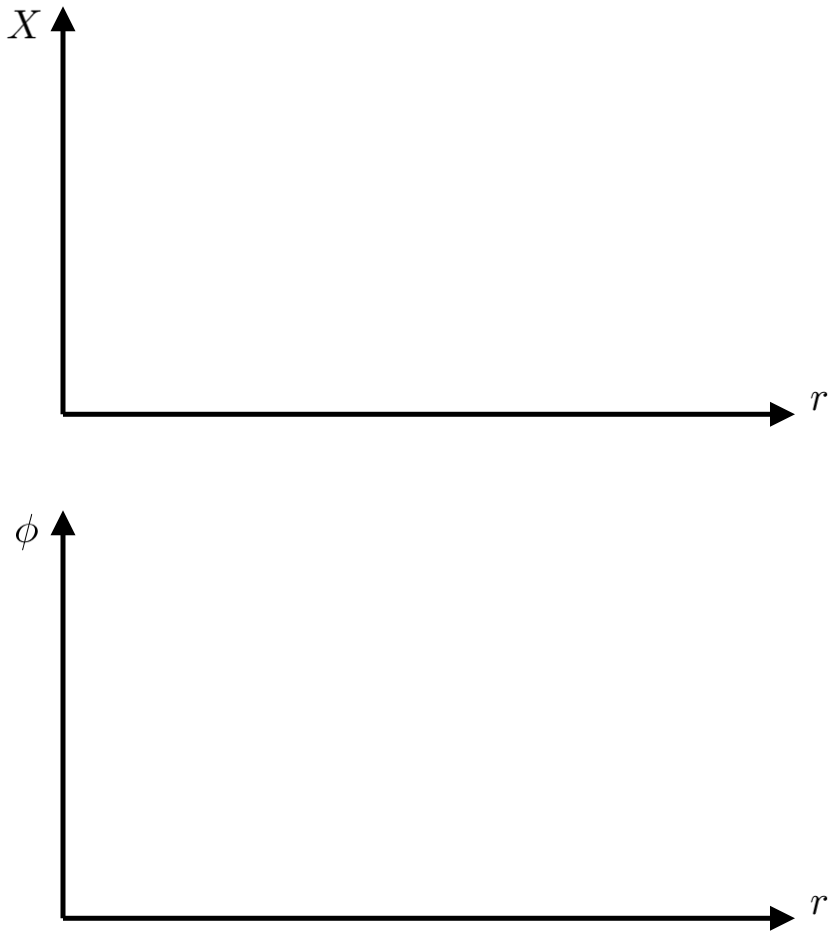
X
r
ϕ
r

Chapter 5

Mechanical Modeling: Multi-Degree-of-Freedom Resonators

5.1 Mechanical Resonators: A Review of Lumped-Mass Modeling and Analysis

The previous chapter investigated the behavior of SDOF resonators, such as those commonly used in resonant mass sensing applications. This chapter extends the aforementioned results to multi-degree-of-freedom (MDOF) systems, which are rapidly emerging as the foundation of microscale RF signal filters, multi-analyte sensors, and microscale data storage systems.

In a generic sense, the systems of interest can be modeled as coupled mass-spring-dashpot systems.

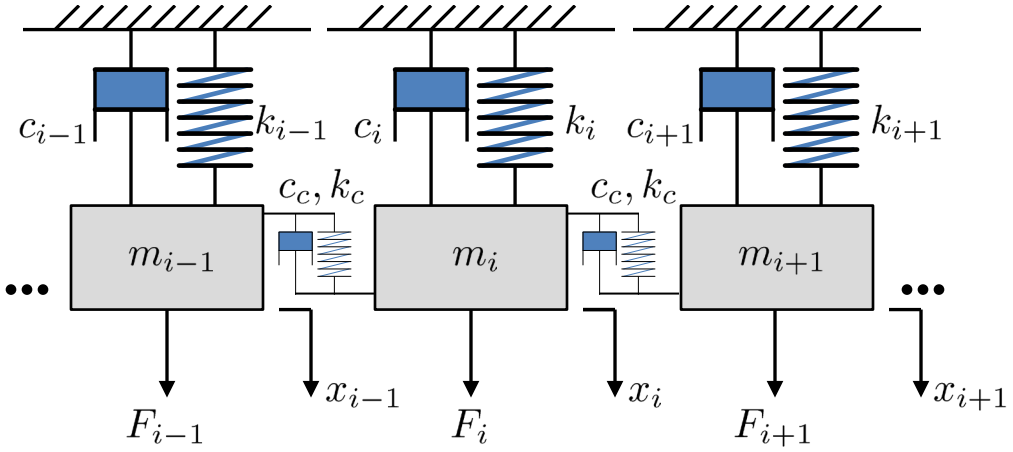

Applying Newton's Second Law:

(5.1)

This and most other coupled mass-spring-dashpot systems can be represented in matrix form as:

$$\mathbf{M}\ddot{\mathbf{x}} + \mathbf{C}\dot{\mathbf{x}} + \mathbf{K}\mathbf{x} = \mathbf{F}(t), \tag{5.2}$$

where for this system:

(5.3)

(5.4)

(5.5)

(5.6)

(5.7)

5.1.1 Natural Frequencies and Mode Shapes

As with the SDOF example considered in the previous chapter, the MDOF system examined here has certain natural frequencies which it *likes* to vibrate at. These can be recovered by following a procedure analogous to that we previously considered.

The natural frequencies of the MDOF system can be recovered from the undamped system:

$$\mathbf{M}\ddot{\mathbf{x}} + \mathbf{K}\mathbf{x} = \mathbf{0}. \tag{5.8}$$

Assuming,

(5.9)

and substituting, yields:

(5.10)

For there to be a non-trivial solution to this equation

(5.11)

Solving this expression for the roots ω_i yields the system's *natural frequencies*. Likewise, solving the associated eigenvector problem

(5.12)

yields the system's *mode shapes*. From these two quantities one can recover the system's free response (presuming the system is undamped)! The analysis of damped free response is omitted here, as it is rarely important in MEMS/NEMS contexts.

5.1.2 Forced Vibration of a Multi-Degree-of-Freedom System

For the SDOF system considered in the previous module the forcing was assumed to be harmonic to facilitate ease of analysis. This section adopts a similar approach, but adopts a complex notation, as it allows the effects of dissipation to be included.

Recall:

$$\mathbf{M}\ddot{\mathbf{x}} + \mathbf{C}\dot{\mathbf{x}} + \mathbf{K}\mathbf{x} = \mathbf{F}(t), \tag{5.13}$$

Assume $\mathbf{F}(t)$ is harmonic:

(5.14)

then

(5.15)

where $\mathbf{B}$ is a complex-valued vector.

Differentiating $\mathbf{x}(t)$ yields:

(5.16)

Substituting these expressions into the equation of motion yields:

(5.17)

(5.18)

It proves convenient to introduce a complex impedance matrix $\mathbf{Z}$, this yields:

(5.19)

Inverting yields an expression **B**

(5.20)

and thus a closed-form solution for the amplitude and phase of the harmonic response!

Example 5.1

Given: Consider a three-resonator, ladder filter comprised of identical MEMS resonators. In this system $k_i = 0.25$ N/m, $m_i = 100$ pg, $k_c = 0.0025$ N/m. Damping is assumed to be negligible.

Find:
(a) The natural frequencies of the system.
(b) The system's frequency response if a unit sine wave input is added to the first element.

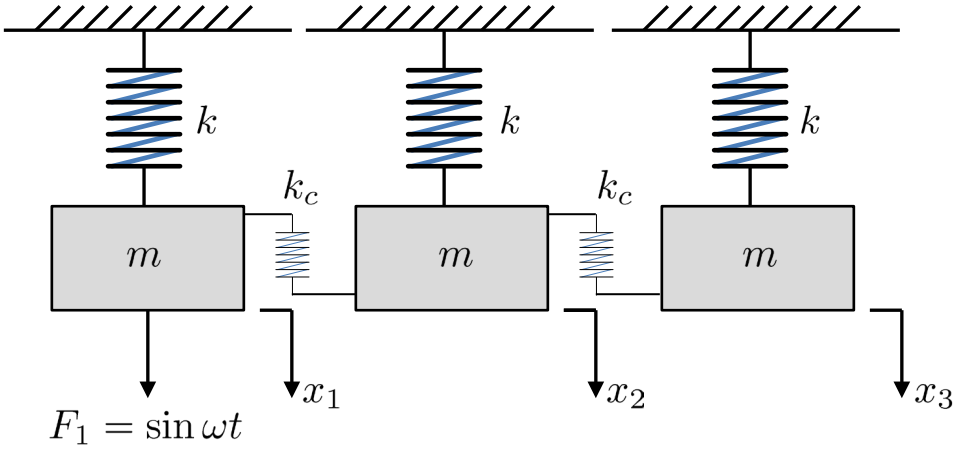

Chapter 6

Mechanical Modeling: Continuous System Resonators

6.1 Free Vibration of Continuous Systems

The previous modules consider the dynamic behavior of single- and multi-degree-of-freedom resonant systems. This module seeks to build upon those results by examining the response of resonators modeled as continuous systems. This response is relatively easy to recover, provided care is taken to convert the governing partial differential equation (PDE) into a set of ordinary differential equations (ODEs). To demonstrate how the dynamic response of continuous systems can be analyzed, the present module adopts a case study approach similar in form to that presented in [11].

Consider the equation of motion governing the undamped, transverse deflections of a uniform, thin beam:

(6.1)

Here, E represents the beam's modulus of elasticity, I is the cross-sectional area moment of inertia, ρ details the beam's mass density, and A is the beam's cross-sectional area. This can be rewritten as

(6.2)

where

$$c = \sqrt{\frac{EI}{\rho A}} \tag{6.3}$$

The free vibration of this system can be recovered via separation of variables:

(6.4)

Substituting:

(6.5)

Since the left and right hand sides of this equation depend on independent variables, ω must be constant. Accordingly,

(6.6)

(6.7)

where

$$\beta^4 = \frac{\omega^2}{c^2} = \frac{\rho A \omega^2}{EI} \tag{6.8}$$

The temporal ODE can be solved using techniques introduced in prior modules:

(6.9)

where A_1 and B_1 are constants determined through the application of initial conditions.

The spatial ODE can be solved by assuming the solution has a form given by:

(6.10)

Substituting this results yields:

(6.11)

which in turn gives an explicit form for $W(x)$:

(6.12)

The natural frequencies of the system can be recovered from:

(6.13)

Note that there are an infinite number of solutions (and thus an infinite number of natural frequencies and corresponding mode shapes) for this system! The ith natural frequency ω_i and the corresponding modeshape $W_i(x)$ can be used to recover the total response:

$$w(x,t) = \sum_{i=1}^{\infty} W_i(x) \left(A_i \cos \omega_i t + B_i \sin \omega_i t \right) \tag{6.14}$$

Note that A_i and B_i are constants fixed by the system's initial conditions. Finally, note that in most MEMS/NEMS devices, a single or few mode shape approximation for $w(x,t)$ suffices.

6.2 Recovering the Natural Frequencies and Mode Shapes of Uniform Beams

The equations developed in the previous section provide closed-form expressions for $W_i(x)$ and ω_i (the beam's mode shapes and natural frequencies) which are completely specified, except for a small number of constants. These values can be explicitly recovered through the application of boundary conditions.

Consider, for example, a fixed-fixed beam of length l without an applied axial load. The boundary conditions for this system can be expressed as:

(6.15)

Recall Equation (6.12):

$$W(x) = C_1 \cos \beta x + C_2 \sin \beta x + C_3 \cosh \beta x + C_4 \sinh \beta x \tag{6.16}$$

It proves convenient to rewrite this as:

(6.17)

Enforcing the boundary conditions yields:

(6.18)

(6.19)

(6.20)

For there to be a non-trivial solution to these equations:

(6.21)

This yields:

$$\cos\beta l \cosh\beta l - 1 = 0 \tag{6.22}$$

Clearly, this equation is satisfied for multiple values of β and thus multiple values of ω. These are the natural frequencies of the system ω_i!

Note that the constant $\hat{C}_4$ can be expressed in terms of $\hat{C}_2$. This yields:

(6.23)

Substituting this result in $W_i(x)$ yields:

(6.24)

which, in turn, yields:

(6.25)

Summing over all of the system's modes yields:

$$\begin{aligned} w(x,t) &= \sum_{i=1}^{\infty} w_i(x,t) \\ &= \sum_{i=1}^{\infty} \left[(\cos\beta_i x - \cosh\beta_i x) - \frac{\cos\beta_i l - \cosh\beta_i l}{\sin\beta_i l - \sinh\beta_i l} (\sin\beta_i x - \sinh\beta_i x) \right] \\ &\qquad \times (A_i \cos\omega_i t + B_i \sin\omega_i t) \end{aligned} \tag{6.26}$$

where A_i and B_i are recovered from the system's initial conditions.

Note that this procedure is easily extrapolated to more complex systems and boundary conditions!

It should also be noted that for the vast majority of mechanical and electromechanical systems, any two mode shapes $W_i(x)$ and $W_j(x)$ will be orthogonal. More specifically,

(6.27)

This along with mass normalization, specifically,

(6.28)

proves very helpful in analysis.

6.3 An Alternate Approach for Characterizing Free Vibration Responses of Continuous Systems

Earlier in this module, the solution to the classical, undamped beam vibration problem was recovered through variable separation. In particular,

(6.29)

Substituting this into the equation of motion of a freely-vibrating beam without an applied axial load results in:

(6.30)

This equation can be *projected* onto a specific mode by multiplying the equation by $W_j(x)$ and integrating over the length of the beam l. This eliminates an explicit spatial dependency:

(6.31)

Applying the orthogonality conditions presented in the previous section yields:

(6.32)

where $\eta_i(t)$ is the ith modal coordinate and ω_i is the system's ith natural frequency. This equation is, in essence, the equation of motion for a single-degree-of-freedom system!

Solving the equation detailed above yields:

(6.33)

with initial conditions given by

(6.34)

(6.35)

where

$$w(x,0) = w_0(x) \tag{6.36}$$

and

$$\frac{\partial w}{\partial t}|_{(x,0)} = \dot{w}_0(x) \tag{6.37}$$

These can be substituted into Equation (6.29) to obtain $w(x,t)$ in an exact or approximate form.

6.4 Forced Vibration of Continuous Systems

The methods presented in this module, thus far, are appropriate for characterizing the free response, natural frequencies, and mode shapes of a continuous system. However, most MEMS and NEMS are forced systems. Luckily, these forced systems can be analyzed using analogous techniques.

Consider the harmonically forced version of the equation of motion initially considered in this module:

(6.38)

As before, let

(6.39)

where $W_i(x)$ are recovered from

(6.40)

Substituting yields:

(6.41)

Combining the above results renders:

(6.42)

Projecting the result on a single mode yields:

(6.43)

This can be rewritten as:

(6.44)

where

(6.45)

are the applied generalized forces.

Solving this new equation of motion (via convolution) yields:

(6.46)

which in turn yields:

$$w(x,t) = \sum_{i=1}^{\infty} \left[A_i \cos \omega_i t + B_i \sin \omega_i t + \frac{1}{\omega_i} \int_0^t Q_i(\tau) \sin \omega_i (t-\tau) d\tau \right] W_i(x) \tag{6.47}$$

Note that as before, these methods can be easily extended to plate- or membrane-like structures.

Example 6.1

Given: Consider a thin uniform beam with modulus of elasticity E, mass density ρ, cross-sectional area A, and cross-sectional area moment of inertia I. Assume the beam is 1 m long and clamped at both ends.

Find:
(a) Determine the natural frequencies of the system as function of the given variables.
(b) Find and plot the system's first four mode shapes.

Example 6.2

Given: Consider a thin uniform beam of length L with modulus of elasticity E, mass density ρ, cross-sectionalal area A, and cross-section area moment of inertia I. A concentrated harmonic load is applied to the beam at a position $x = a$. That is, $f(x,t) = F_0 \sin \omega t \delta(x-a)$.

Find: An expresion for the deflection of the beam $w(x,t)$ assuming arbitrary boundary conditions and zero initial conditions.

Chapter 7

Electrostatic Transduction: Parallel-Plate Systems

7.1 Maxwell's Equations

Thus far, this lecturebook has focused on the modeling and subsequent analysis of elastic structures. Here, the focus shifts to various transduction mechanisms, as the combination of mechanical modeling/analysis and transduction modeling/analysis forms the basis for true MEMS/NEMS modeling/analysis.

This module specifically focuses on electrostatic transduction, given its prevalence in many MEMS and NEMS devices. Though the base-level models for electrostatic forces are well known, in the spirit of thoroughness, the module will begin with a review of Maxwell's Equations.

Maxwell's Equations:

(7.1)

(7.2)

(7.3)

(7.4)

where the vector differential operator $\vec{\nabla}$ is given by

(7.5)

$\vec{\mathcal{E}}$ is the electric field, $\vec{B}$ is the magnetic field (or, more accurately, magnetic flux density), $\vec{D}$ is the electric displacement field (or, more accurately, electric flux density), $\vec{H}$ is the magnetizing field, ρ

is the total charge density, $\vec{J}$ is the current density, and c is the speed of light in vacuum.

Given the interest here is in electrostatics,

$$\frac{\partial \vec{B}}{\partial t} = \frac{\partial \vec{D}}{\partial t} = \vec{0}. \tag{7.6}$$

This, assuming the current density $\vec{J} = 0$, yields:

(7.7)

(7.8)

Equation (7.7) yields

(7.9)

namely, that $\vec{E}$ is the gradient of a potential function. This, in turn, yields

$$\nabla^2 \phi = \frac{\rho}{\varepsilon_0} \tag{7.10}$$

where ε_0 is the permittivity of free space, provided the system material of interest is approximately homogeneous and isotropic (i.e. $\vec{D} = \varepsilon_0 \vec{\mathcal{E}}$).

Equation (7.9), which is known as Poisson's equation, forms the basis of most electrostatics problems!

7.2 Parallel-Plate Systems

To full analyze parallel-plate systems, it helps to use the integral form of Gauss' Law

(7.11)

where q is the total charge enclosed by S and $\hat{n}$ is a unit normal to the surface. Consider this equation in the context of the parallel-plate system shown below:

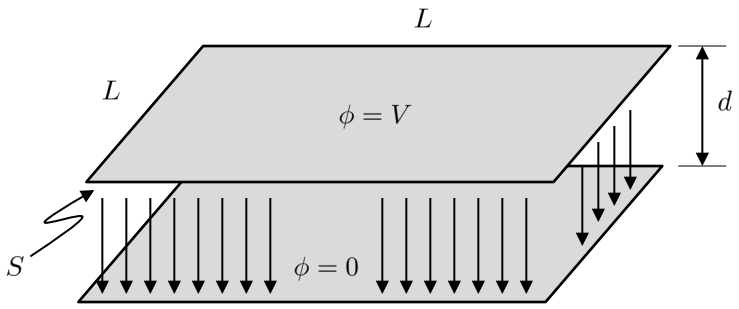

where d is the gap between plates, L is the plate's edge length, and ϕ is the applied voltage potential.

(7.12)

Here,

(7.13)

(7.14)

Therefore,

(7.15)

where A is the area of the plate. Substituting this result into the integral form of Gauss' Law yields:

(7.16)

From the differential form of Gauss' Law:

(7.17)

Also, recall that the charge stored in a capacitor $Q = CV$, where C is the device's capacitance. Taken together, this yields:

(7.18)

This can be generalized to allow for an arbitrary medium between the plates as:

$$C = \frac{\varepsilon A}{d}, \tag{7.19}$$

where ε is the permittivity of the gap medium.

7.3 Electrostatic, Parallel-Plate Actuation (Variable Gap)

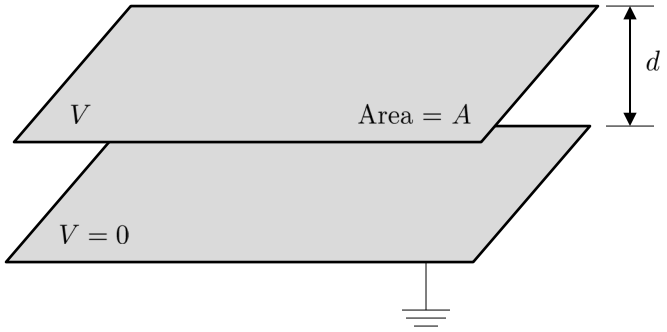

Recall the definition of capacitance developed in the previous section for the parallel-plate system shown above:

$$C = \frac{\varepsilon A}{d}. \tag{7.20}$$

If the gap parameter d is altered, an *attractive* force is generated.

Recall that the total energy stored in a capacitor U is given by:

(7.21)

The force is then given by

$$F = -\frac{\partial U}{\partial x} = -\frac{1}{2}\frac{\partial C}{\partial x}V^2, \tag{7.22}$$

where x is the displacement variable of interest.

For a variable-gap, parallel-plate system, this yields:

(7.23)

7.4 Electrostatic, Parallel-Plate Sensing (Variable Gap)

The previous section detailed how parallel-plate structures can be used for actuation purposes. Since electrostatics is a true transduction mechanism, it is also very useful for sensing. Specifically, by exploiting electrostatic effects, a change in capacitance can be used to measure a change in displacement.

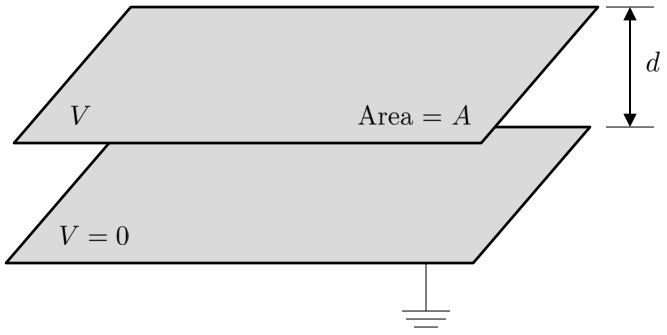

Recall that the capacitance associated with the parallel-plate system shown above is given by:

(7.24)

If an external effect induces a change in the gap δd, then

(7.25)

If δd is small, this yields:

(7.26)

which, in turn, yields:

$$\Delta d \approx -\frac{\Delta C d^2}{\varepsilon A}. \tag{7.27}$$

Note that in practice, measuring small displacement-induced changes in capacitance (commonly sub-pF) can be exceedingly difficult. Fortunately, a number of integrated circuit (IC) companies, such as Analog Devices, have developed custom electronics specifically oriented for this task.

7.5 A Note on Fringing Fields

The previously introduced capacitance model relies heavily on the assumption that $d << L$. That is, that the gap width is appreciably smaller than the length and width of the capacitive element. However, this approximation does not always suffice. In many scenarios fringing fields must be accounted for.

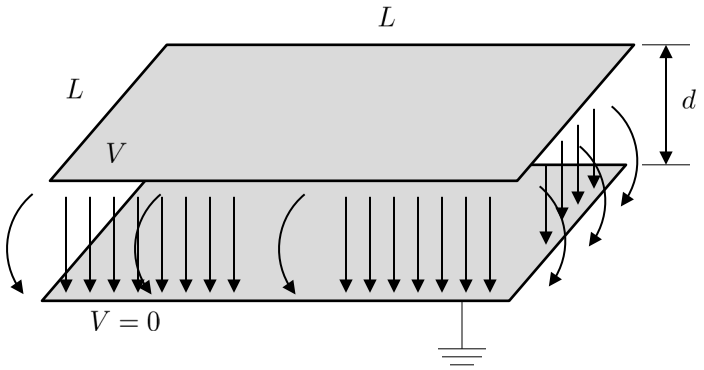

In these scenarios a modified capacitance of the form

$$C = \frac{\varepsilon A}{d} + \frac{2\varepsilon L}{\pi} \ln\left(\frac{L\pi}{d}\right) \tag{7.28}$$

is often used. Similar results exist for rectangular plates, as well as many other geometries.

7.6 Electrostatic Pull-In

One interesting phenomenon that can occur in variable-gap, electrostatically-transduced systems is *pull-in*. Pull-in describes the electromechanical state wherein the net electrostatic forces on a given system exceed the mechanical restoring forces, which, in turn, leads to the collapse of the system's upper electrode (typically the mechanical structure) onto the system's lower electrode (typically a metalized substrate). In systems such as RF switches, this phenomenon can be beneficially leveraged. However, in many applications pull-in will represent a practical design constraint. To analyze this phenomenon in depth, consider the single-degree-of-freedom electromechanical system shown below.

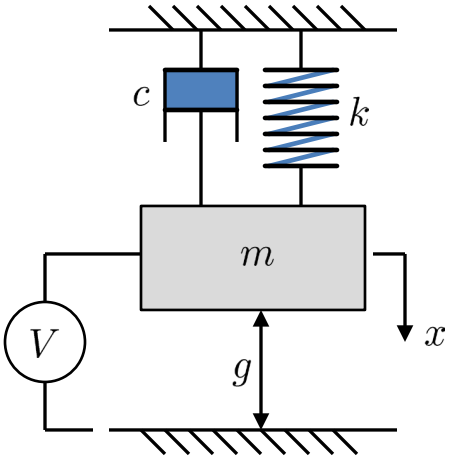

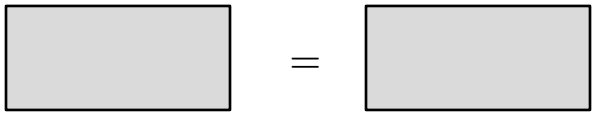

Applying Newton's Second Law yields:

(7.29)

where A is surface area of the electrodes, ε is permittivity of the gap medium, and all other parameters are defined as in the figure.

Expanding the right hand side of this equation in a Taylor Series assuming $x << g$ renders:

$$\frac{\varepsilon A V^2}{2(g-x)^2} \approx \frac{\varepsilon A V^2}{2}\left[\frac{1}{g^2} + \frac{2}{g^3}x + \frac{3}{g^4}x^2 + ...\right] \tag{7.30}$$

Retaining linear terms in the displacement variable x yields:

(7.31)

If V was a harmonic function, this equation of motion could be analyzed using previously-introduced techniques (provided the second term on the right hand side was omitted). If V is a DC voltage the static pull-in behavior can be approximated using this equation (*Is there an intrinsic problem with this?*), or by reverting to the unexpanded model.

Key Result: Consider the unexpanded equation of motion detailed below:

$$m\ddot{x} + c\dot{x} + kx = \frac{\varepsilon A V^2}{2(g-x)^2} \tag{7.32}$$

Limiting the scope of this analysis to static behavior yields:

(7.33)

This can be rewritten as:

(7.34)

Solving this equation for x yields the following characteristic, where

(7.35)

and

(7.36)

Point PI on this figure is the *static pull-in* point. Above this DC excitation voltage, the system does not exhibit a stable equilibrium and the mass collapses onto the bottom electrode!

Note that there is an analogous dynamic phenomenon called *dynamic pull-in*. In this scenario, the device collapses onto the substrate under the influence of a dynamic voltage excitation. The pull-in voltage associated with dynamic collapse can be greater than, less than, or equal to the static pull-in condition. Accordingly, particular care must be taken during design.

Example 7.1

Given: Consider a thin uniform beam with modulus of elasticity E, mass density ρ, cross-sectional area A, and cross-sectional area moment of inertia I. Assume the beam is L long, b wide, clamped at both ends, and electrostatically-actuated by an electrode spanning the beam's entire length.

Find:
(a) Find a linear, lumped-mass representation of the system.
(b) Find the static pull-in voltage predicted by the system model.
(c) Comment on any potential sources of discrepancy which may lead to erroneous pull-in predictions.

Chapter 8

Electrostatic Transduction: Comb Drives and Tuning Mechanisms

8.1 Interdigitated Comb Drives

Electrostatic comb drives leverage arrays of finger-like geometries to develop displacement-dependent capacitances which can be exploited in uniaxial sensing or actuation. In the traditional form, so-called *interdigitated comb drives*, the fingers overlap, as shown below.

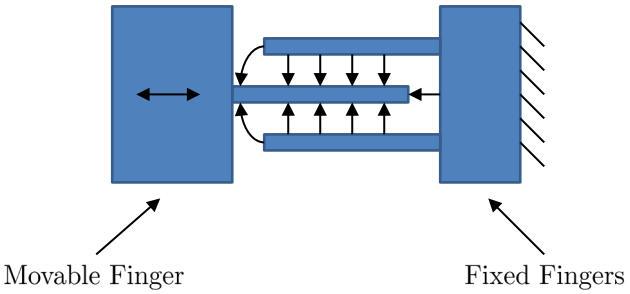

Displacement-induced capacitive changes in this system can derive from two effects: (i) variable gaps (in multiple places) and (ii) variable overlap areas. Traditionally, the variable overlap area characteristic is exploited for transduction.

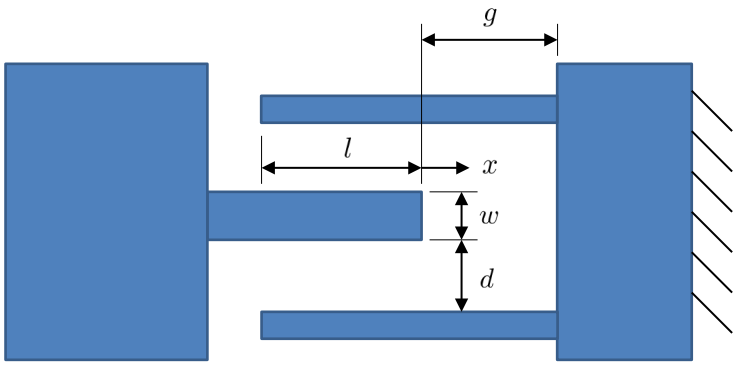

The capacitance associated with the system shown above can be written as [10]:

(8.1)

where C_{ff} is the capacitance contribution attributable to fringing electric fields, h is the thickness of the comb drive actuator, ε is the permittivity of the gap medium and all other parameters are defined as in the above figure.

8.1.1 Actuation using Interdigitated Comb Drives

Recall that an attractive electrostatic force can be computed from a system's capacitance C using:

$$F = -\frac{1}{2}\frac{\partial C}{\partial x}V^2 \tag{8.2}$$

where V is the potential difference between the capacitor's electrodes and x is the displacement variable of interest.

For the system shown above this yields:

(8.3)

which is commonly written as a positive quantity (it is attractive in nature)

(8.4)

This equation is a good approximation for the total electrostatic force, provided the system capacitance does not change appreciably with x (i.e. there is sufficient gap g).

Extending this result to an N interaction comb drive yields:

(8.5)

where N is the total number of comb interactions.

Note that recent work has accounted for the effect of the electric fringe fields as well. Though it is yet to be experimentally validated, the predicted electrostatic force for a single comb pair can be expressed as:

$$F = \frac{V}{2}\left\{2\varepsilon\frac{V}{\pi}\left[\ln\left(\left(\left(\frac{w}{d}+1\right)^2-1\right)\left(1+\frac{2d}{w}\right)^{1+w/d}\right)+\frac{2\pi h}{d}\right]\right\}-2\left(d+w\right)\frac{\varepsilon V^2}{2\pi l}. \tag{8.6}$$

Given the complexity of this forcing, the remainder of the lecturebook will leverage the simplified force model.

Key Result: Before proceeding, there are a few notes worth making. Interdigitated comb drives:

- Yield a linear force, which is independent of the displacement variable of interest.
- Facilitate a long range of planar travel.
- Are difficult to fabricate.
- Generate a comparatively-small force (see Example 8.1 for further details).

8.1.2 Sensing using Interdigitated Comb Drives

Much like their parallel-plate counterparts, interdigitated comb drives are also suitable for sensing purposes.

Recall that the capacitance of a single comb pair is given by:

$$C = \frac{2\varepsilon h(l+x)}{d} + C_{ff} \tag{8.7}$$

The partial derivative of the capacitance with respect to the displacement variable x is thus:

(8.8)

Provided the displacement is small in comparison to the total finger length, this can be approximated as:

(8.9)

which yields:

(8.10)

8.2 Non-Interdigitated Comb Drives

Though the interdigitated comb drives detailed in the previous sections provide transduction in the vast majority of comb-based microsystems, recently a number of applications have turned toward their non-interdigitated counterpart shown below.

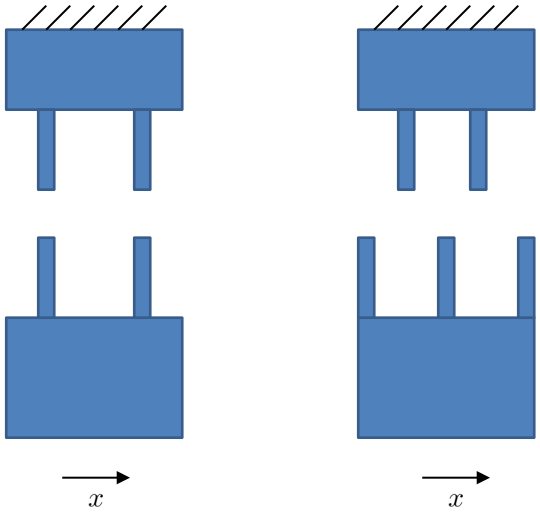

Augmentation Drive Reduction Drive

This type of drive provides motion in the indicated x direction via a force of the form:

$$F \approx f(x)V^2 \approx \left(r_1 x + r_3 x^3\right) V^2. \tag{8.11}$$

As quick analysis reveals, this force is proportional to x and x^3 and thus is actually a modulation of the system's stiffness. This form of excitation is called a *parametric excitation*.

Though it was not previously discussed, a similar excitation was seen during the Taylor Series expansion of the variable-gap electrostatic force:

$$F = \frac{\varepsilon A V^2}{2(g-x)^2} \approx \frac{\varepsilon A V^2}{2}\left[\frac{1}{g^2} + \frac{2}{g^3}x + \frac{3}{g^4}x^2 + ...\right] \tag{8.12}$$

While the analysis of excitations such as these are largely beyond the scope of this class, suffice it to note that parametric excitations are now being routinely exploited in resonant MEMS/NEMS to recover superior frequency response characteristics. The instructor has extensive experience with these systems and is happy to answer any further questions you have in this regard.

8.3 Tuning Mechanisms

Before finalizing this lecturebook's discussion of electrostatic transduction, it is prudent to briefly discuss one of the inherent advantages of electrostatic actuation that is commonly overlooked: *stiffness* and *frequency tuning*. To investigate these phenomena, consider the generic lumped-mass model for an electrostatically-actuated micro- or nanosystem shown below:

(8.13)

Here, m_{eff}, c_{eff} and k_{nom} represent the system's effective mass, effective damping, and nominal stiffness, α and β are dimensional constants, N is an applied axial force (e.g. that generated due to residual stress in a fixed-fixed beam), and $f(V^2)$ accounts for a portion of the applied electrostatic force (the rest being accounted for by the βV^2 or neglected as a higher-order contribution).

Using the above equation as reference, it proves useful to define an effective stiffness k_{eff}:

(8.14)

In general, $\alpha > 0$ and $\beta < 0$, thus:

- Increasing N, increases the effective stiffness. This can be done by designing the system appropriately (e.g. predetermining the post-fabrication intrinsic stress). Likewise, decreasing N, decreases the effective stiffness. This can be done by designing the system appropriately (e.g. by adding local heating elements).
- Increasing V, decreases the effective stiffness. That is, by increasing the applied potential, the *electrostatic stiffness* will partially negate the nominal mechanical stiffness.

Recalling that

(8.15)

it can also be noted that:

- Increasing N or decreasing V, increases the natural frequency ω_n.
- Decreasing N or increasing V, decreases the natural frequency ω_n.

These mechanisms are exploited extensively in practical application.

Example 8.1

Given: Consider a 100 interaction comb drive of thickness $h = 5$ μm with a gap $d = 2$ μm and an applied actuation voltage of $V = 20$ V.

Find:
(a) Find the magnitude of the net electrostatic force.
(b) Estimate the *overlap area* and *total planar area* consumed by the actuator if the finger length $L = 10$ μm (assumed to all be equal), the finger overlap $l = 5$ μm, and the finger width $w = 2$ μm.
(c) Compare the generated force to that produced by a parallel-plate electrostatic transducer with the same *overlap area* and gap.
(d) Compare the generated force to that produced by a parallel-plate electrostatic transducer with the same *total planar area* and gap.

Chapter 9

Piezoresistive Sensing

9.1 Overview

Though electrostatic transduction remains the dominant actuation and sensing mechanisms employed in micro- and nanosystems, a number of research and industrial efforts over the past decade have sought favorable alternatives. Prime examples of such investigations are those focusing on piezoresistive and piezoelectric transduction, transduction mechanisms which mimic electrostatic transduction in the sense that they lead to a coupling (directly or indirectly) between mechanical and electrical fields.

The present module focuses on *piezoresistive transduction*, or more specifically piezoresistive sensing, since the transduction mechanism cannot be used for actuation purposes. This form of sensing exploits the fact that a structure's electrical resistance changes under the influence of a mechanical stress/strain. Though the extent of the piezoresistive effect varies between materials, the fact that it exists in most common materials used in micro/nanofabrication makes it quite appealing. Please note that much of the material presented here derives from Reference [10].

Key Result: Before proceeding, it is prudent to note the benefits and drawbacks of this sensing approach:

- Benefits:
  - Piezoresistive sensing is easy to implement in device designs.
  - Piezoresistive devices are relatively easy to package.
  - Piezoresistive devices are relatively easy to measure.
- Drawbacks:
  - Piezoresistive devices are generally noisy.
  - Piezoresistive devices exhibit a notable temperature dependence.
  - Piezoresistive devices are power consuming.

9.2 Modeling Basics

Recall that the resistance of a bar of material is given by:

(9.1)

where ρ is the resistivity of the material, A is the cross-sectional area of the bar, and L is the length of the bar.

A small, fractional change in resistance can thus be expressed as:

(9.2)

Namely, a combination of material and geometric effects.

The change in resistivity due to stress is captured by a piezoresistive coefficient:

(9.3)

where σ is the uniaxial stress in the bar, ε is the uniaxial strain in the bar, and E is the material's modulus of elasticity.

Furthermore, the fractional change in resistance due to strain is captured by a gage factor GF:

(9.4)

Noting that uniaxial strain is defined as:

(9.5)

and that

(9.6)

where ν is the Poisson's ratio of the material, yields:

(9.7)

Given that for the majority of materials, Poisson's ratio is between 0 and 0.5, purely mechanical gage factors are typically between 1 and 2 (this is true for most metals, as an example). However, the gage factors of semiconductors are often 1-2 orders of magnitude greater, making piezoresitive effects an appealing transduction mechanism in semiconductor systems.

9.3 Piezoresistance in Silicon

The coefficients which govern the piezoresistance of anisotroic materials, such as silicon, depend on both microstructure and crystal orientation.

While generic scenarios can be considered, the two most practical sensing schemes in such materials are those wherein the stress is in the direction of the current σ_l and/or transverse to the current σ_t. In these cases:

(9.8)

where π_l and π_t are piezoresistive coefficients obtained from experimental data.

For the sake of reference, these piezoresistive coefficients for silicon are given in the tables below.

n-Type Doping			
Orientation	[1 0 0]	[1 1 0]	[1 1 1]
π_l (10^{-11}/Pa)	-102.2	-31.2	-7.5
π_t (10^{-11}/Pa)	53.4	-17.6	6.1
p-Type Doping			
Orientation	[1 0 0]	[1 1 0]	[1 1 1]
π_l (10^{-11}/Pa)	6.6	71.8	93.5
π_t (10^{-11}/Pa)	-1.1	-66.3	44.6

Please note that the above coefficients have a strong temperature dependence. If the doping concentration within the silicon is sufficiently low, this temperature dependence can be approximated by:

(9.9)

Note that though these temperature effects can present a daunting challenge, ratiometric measurements can overcome some degree of temperature dependence. Accordingly, resistive changes

due to piezoresistive effects are commonly measured by bridge circuits. Unfortunately, these often consume appreciable DC power.

9.4 Piezoresistance in Isotropic Materials

Many isotropic semiconductors have gage factors in the 10s or 100s. To calculate piezoresistive coefficients for these materials, it is typically safe to assume that

(9.10)

Example 9.1

Given: Consider a piezoresistor of length $L = 50$ μm, cross-sectional area $A = 20$ μm^2, resistivity $\rho = 0.02$ Ωm in an environment of temperature $T = 300$ K.

Find:
(a) The change in resistance ΔR resulting from a 10 MPa change in longitudinal stress.
(b) The change in resistance ΔR resulting from a 5 K change in temperature.
(c) Determine which effect dominates.

Example 9.2

Given: Consider piezoresistive accelerometer fabricated from a beam of length $L = 200$ μm, thickness $t = 2$ μm and width $b = 10$ μm. Assumed that the piezoresistive element is located at the base of the cantilevered beam and that it can be approximated as an isotropic material with an elastic modulus of $E = 170$ GPa, and $\pi_l = 20 \times 10^{-11}$ Pa^{-1}.

Find: Determine $\Delta R/R$ for this system assuming longitudinal effects dominate.

Chapter 10

Piezoelectric Transduction

10.1 Overview

The *piezoelectric effect* refers to the multiphysical coupling that exists in some materials between the material's mechanical and electrical fields. Note that this mechanism differs from the *piezoresitive effect* discussed in the prior module, because the piezoelectric effect leads to a direct generation of an electric field, rather than simply a change in resistance.

Generally speaking, the piezoelectric effect is described in terms of two processes. The *direct effect of piezoelectricity* describes the fact that certain materials generate an electric field (and thus voltage) when under the influence of a mechanical stress. Likewise, the *inverse effect of piezoelectricity* describes the fact that the same materials produce mechanical deformation (and thus force) when under the influence of an electrical field.

Note that piezoelectric materials are *poled, crystalline materials* such as ZnO, PZT ($PbZrTiO_3$), Quartz, and PVDF.

10.2 Modeling the Piezoelectric Effect

The equation governing the *direct effect of piezoelectricity* is typically given as:

(10.1)

where $\mathbf{D}$ is the electrical displacement (C/m), $\mathbf{d}$ is a piezoelectric coefficient matrix (C/N), $\boldsymbol{\sigma}$ represents the stress field in the material (N/m^2 or Pa), $\boldsymbol{\varepsilon}$ represents the electrical permittivity matrix (F/m), and $\boldsymbol{\mathcal{E}}$ represents the electrical field (V/m).

Expanding this into matrix form yields:

(10.2)

where σ_1 - σ_3 are the normal stresses acting on the piezoelectric crystal, and τ_1 - τ_3 are the shear stresses acting on the crystal respectively. These values are highlighted on the unit stress element shown below.

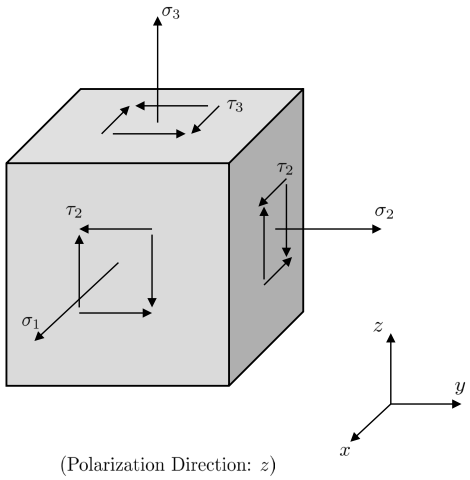

The equation governing the *indirect effect of piezoelectricity* is typically given as:

(10.3)

where $\hat{\varepsilon}$ represents the strain vector associated with the system and $\mathbf{S}$ is the system's compliance matrix.

Expanding this in matrix form yields:

(10.4)

where γ_1 - γ_3 represent shear strains.

While the equation provided above provide some insight on the modeling of piezoelectric effects, they lack a certain transparency with respect to everyday application. In general, these equations are applied under the assumption that dominant piezoelectric effects are uniaxial. This allows a simplified equation of the form:

(10.5)

to be applied, where $E = S^{-1}$ is the modulus of elasticity of the material.

10.3 Lumped-Mass Actuator Models

10.3.1 Longitudinal-Mode Actuators

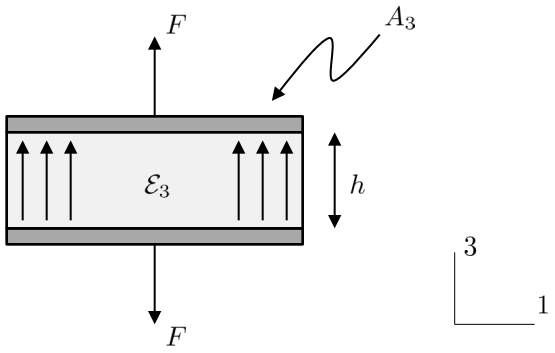

The model for a longitudinal actuator can be developed by rewriting Equation (10.5) as:

(10.6)

where the first term on the right hand side of the equation accounts for material deformation and the second the piezoelectric effect. Though an appreciable amount of physics have been neglected in this simple lumped-mass model, the contributions of the omitted terms are typically quite small.

If the material is free to deform, $\sigma_3 = 0$, this yields:

(10.7)

assuming $V = \mathcal{E}_3 h = \text{constant}$.

In uniaxial situations:

(10.8)

thus,

(10.9)

If a force output proves more meaningful than displacement output, this can be rewritten as:

(10.10)

Note that in contrast to electrostatic forces, this force can be positive or negative!

10.3.2 Transverse-Mode Actuators

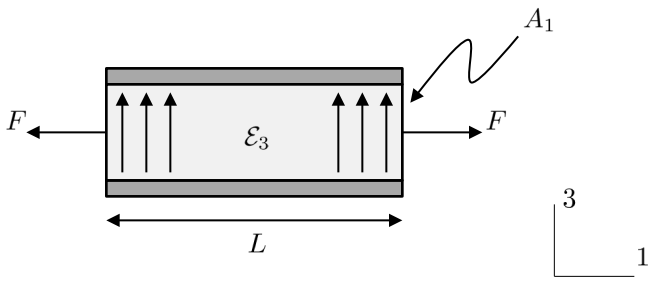

The model for a transverse actuator can be developed by rewriting Equation (10.5) as:

(10.11)

Similar to before, if the material is free to deform, $\sigma_1 = 0$, this yields:

(10.12)

assuming $V = \mathcal{E}_3 h = \text{constant}$.

In uniaxial situations:

(10.13)

thus,

(10.14)

If a force output proves more meaningful than displacement output, this can be rewritten as:

(10.15)

10.4 Lumped-Mass Sensor Models

10.4.1 Longitudinal-Mode Sensors

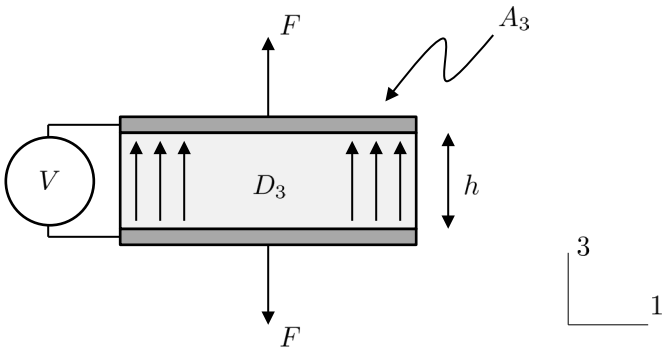

The model for a longitudinal sensor can be developed by rewriting Equation (10.1) as:

(10.16)

Focusing solely on 3-direction dynamics, yields:

(10.17)

Note that this assumes $\hat{\varepsilon}_1 = \hat{\varepsilon}_2 = 0$ and $D_1 = D_2 = 0$.

In uniaxial situations:

(10.18)

where u_3 is the material displacement in the 3-direction at x_3.

Integrating this equation across the sensor yields:

(10.19)

Simplifying this expression renders:

(10.20)

Assuming constant voltage $V = \mathcal{E}_3 h$ yields:

(10.21)

This can be rewritten in terms of charge:

(10.22)

Finally, differentiating this expression yields:

(10.23)

where the first term on the right hand side of the equation represents the AC current passing through the capacitor and the second represents the motional current attributable to the sensor's displacement. Here,

(10.24)

10.4.2 Transverse-Mode Sensors

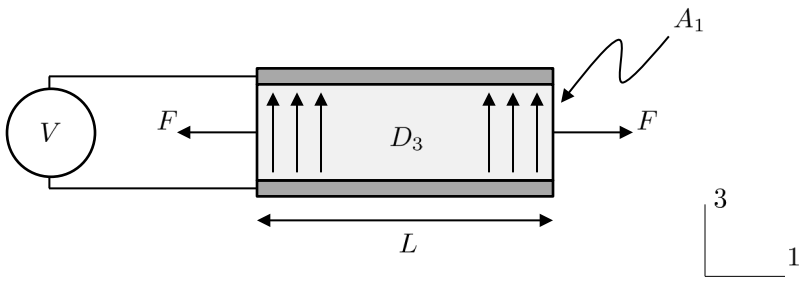

The model for a transverse sensor can be developed by rewriting Equation (10.1) as:

(10.25)

Note that this assumes $\hat{\varepsilon}_2 = \hat{\varepsilon}_3 = 0$ and $D_1 = D_2 = 0$.

In uniaxial situations:

(10.26)

where u_1 is the material displacement in the 1-direction at x_1.

Integrating this equation across the sensor yields:

(10.27)

Simplifying this expression renders:

(10.28)

Assuming constant voltage $V = \mathcal{E}_3 h$ yields:

(10.29)

This can be rewritten in terms of charge:

(10.30)

Finally, differentiating this expression yields:

(10.31)

10.5 A Note on Piezoelectric Transduction in Continuous Systems

Though the present module focused on lumped-mass representation of piezoelectric transducers, this transduction method is often included in continuous system models as well. Interestingly, there are a number of distinct ways this can be done. For example, piezoelectric actuation has been included as a distributed force, distributed moment and internal stress in various research papers.

Example 10.1

Given: Consider the piezoelectric accelerometer shown below. In this system the proof mass m = 0.025 kg, the cross-sectional area of the piezoelectric material is A = 2 cm^2, and $d_{33}E$ = 15.1 C/m^2. The applied acceleration is 1 g in amplitude.

Find: The amount of current i generated if the frequency of the acceleration ω is 1 Hz, 10 Hz, and 100 Hz. Assume the electrical field has a negligible contribution.

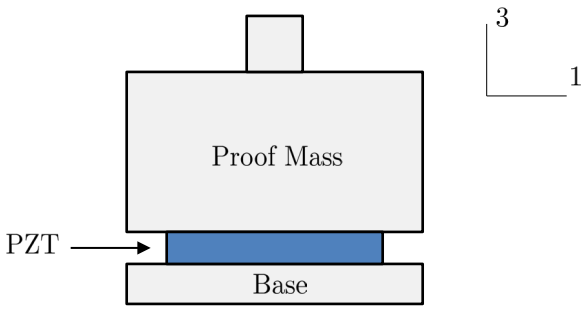

Example 10.2

Given: Consider the single-axis nanopositioner shown below. In this system the cross-sectional area $A_1 = 4\ \mu\text{m}^2$, the stack height $h = 2\ \mu\text{m}$, the length $L = 20\ \mu\text{m}$, and the material has properties: $(d_{33}E)_{PZT}$ = -5.4 C/m^2 and $E_{PZT} = 110$ GPa.

Find:
(a) Find the forced produced by a 20 V excitation.
(b) Determine the level of voltage control needed for 1 nm positioning resolution.
(c) Identify any issues which might hinder positioning.

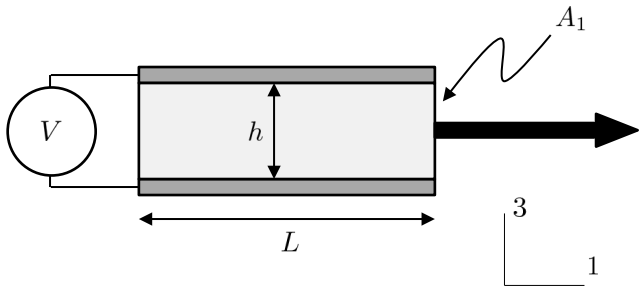

Chapter 11

Magnetic and Electromagnetic Transduction

11.1 The Basics of Magnetism

Unlike electrostatic transduction (and to a lesser extent piezoelectric and piezoresistive transduction), which often lacks efficiency at the macroscale and is thus sparingly used, magnetic and electromagnetic transduction have utility across the entire scale spectrum. Because of this, a macroscale understanding of magnetic and electromagnetic transduction can be applied to micro/nanoscale problems. Here, a modeling and analysis approach akin to that presented in [7] is adopted.

Magnetic materials are composed of magnetic domains, each consisting of a magnetic dipole. If the domains/dipoles have some degree of order, a net magnetic field will be produced.

The *magnetic field intensity*, designated as H and having units (A/m), describes the magnetic influence external to a magnetic material.

The *magnetic field density*, designated as B and having units (T = Wb/m^2 = Vs/m^2), describes the total magnetic field inside of a magnetic material. This accounts for both the induction field and internal magnetization. Note that common ferromagnetic materials typically have magnetic field densities on the order of 0.01 - 0.1 T, and so-called rare earth magnets have magnetic field densities on the order of 1 - 10 T.

The magnetic field intensity and density are related by:

(11.1)

where μ_0 is the magnetic permeability of space (Wb/Am), μ_r is the relative permeability of the material, M represent internal magnetism, and $\chi = \mu_r - 1$ represents the magnetic susceptibility.

Materials with weak, negative χ are often referred to as diamagnetic materials. Likewise, materials with weak, positive χ are often referred to as paramagnetic materials. Both of these types of materials have a relative permeability near unity.

Ferromagnetic materials (Fe, Ni, Co, etc.) have large values of μ_r and are commonly used in MEMS/NEMS applications.

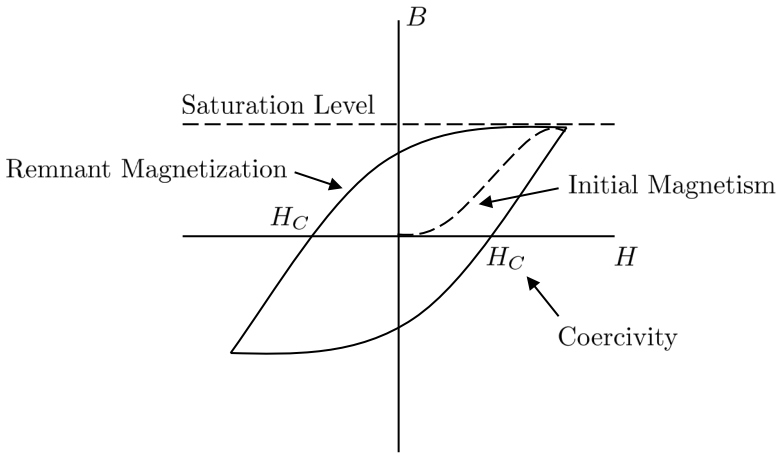

It it important to note that the linear relationship detailed above, is only valid for a limited range of H and B. Across a broader region it is defined by the hysteresis loop shown above. A few features of this diagram are of particular note:

- After an external induction field reaches a certain amplitude, it *saturates*. This corresponds to the field level at which all domains have been aligned.
- Ferromagnetic materials lose some magnetization with the removal of an external field, what is left in H is called *remnance*.
- *Coercivity* is the level of the reserve field required to drive magnetism to zero.
- The area enclosed by the hysteresis loop is a measure of the energy stored in the material.

Finally, it is important to realize that there are two classes of ferromagnets:

- *Hard magnets* retain polarization even under zero magnetic driving field.
- *Soft magnets* exhibit very low remnance and feature internal magnetism only in the presence of an external field.

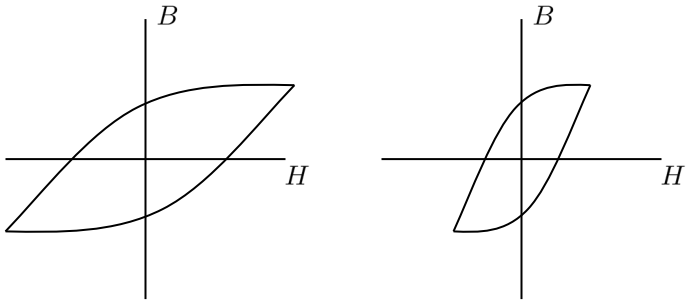

Hard Magnet Soft Magnet

11.2 Actuation via Permanent Magnet Interactions

One form of magnetic transduction involves the use of interactions between a permanent magnet and an external magnetic field for actuation. This type of actuation is akin to that utilized in a simple magnetic compass.

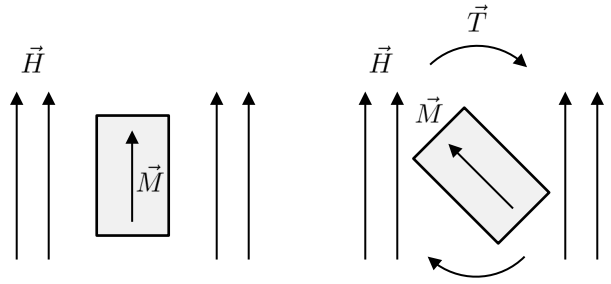

No Force, No Torque No Force, Torque

In this planar scenario, the net torque acting on the system of interest is given by:

(11.2)

where $\vec{M}$ is the magnetization, $\vec{H}$ is the external field and V_{mag} is the magnet volume.

While the uniform magnetic fields utilized above generated solely an actuation moment, non-uniform fields can be exploited to produce both forces and moments.

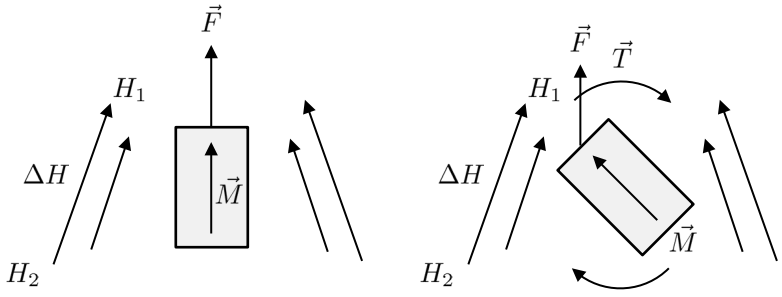

Force, No Torque Force, Torque

Assuming each piece contains two monopoles of opposite polarity:

(11.3)

where A represents the cross-sectional area of the magnet, ΔH represents the change in field, and Δl represent the effective length of the magnet.

11.3 Actuation via Lorentz Forces

The previous section examined the potential for magnetic actuation realized through the interaction between a magnet and an external magnetic field, an alternate approach to magnetic actuation is to utilize electromagnetic interactions to generate a *Lorentz Force*. This is sometimes referred to as *magnetomotive actuation*.

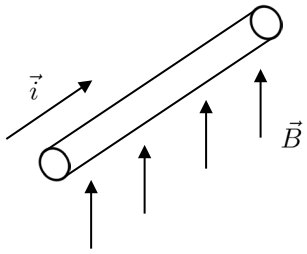

The Lorentz Force resulting from a single charge can be written as:

(11.4)

where q is the charge, $\vec{v}$ is the charge velocity, and $\vec{B}$ is the magnetic field density.

This single charge model can be extended to develop an expression for the Lorentz force acting on a current-carrying wire by considering an n charge system. To realize this, recall that a current is defined to be the total number of positive charges moving through a given cross-sectional area in 1 s. Then,

(11.5)

This yields:

(11.6)

where l is the length of the wire.

Substituting this in the single charge force model yields:

(11.7)

here θ is the angle between $\vec{c}$ and $\vec{B}$. Generalizing this results renders:

(11.8)

11.4 Sensing via Back Electromotive Forces

The previous section detailed how the interaction between a current-carrying conductor and external magnetic field could be utilized for actuation purposes, here this mechanism is shown to enable sensing as well.

Consider Faraday's Law:

(11.9)

Here, V_{emf} is the resulting back electromotive force (emf) resulting from a time variation of $\Phi(t)$, the magnetic flux through a surface of interest.

In general,

(11.10)

where $\hat{n}$ is a unit vector normal to the aforementioned surface and dS is a differential surface element.

Accordingly, for most scenarios, this can be re-written as:

(11.11)

where $\vec{v}$ is the velocity of a differential segment of the conductor $d\vec{l}$. This relationship between velocity and induced voltage enables an excellent sensing mechanism.

Example 11.1

Given: Consider the magnetometer shown below. The magnetic field associated with this scenario is given by $\vec{H}$, the magnetism is specified to be $\vec{M}$, the magnet volume is V_{mag} and the torsional stiffness of the system is k_ϕ.

Find: Determine the resulting torsional deflection ϕ.

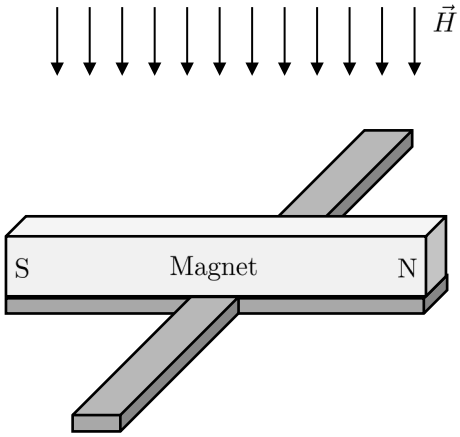

Example 11.2

Given: Consider the magnetomotively-actuated nanowire shown below. Assume that the current passing through the nanowire $i = 1$ μA, the magnetic field density $\vec{B} = 8$ T $\hat{k}$, and the wire length $L = 2.25$ μm.

Find:

(a) Using the techniques presented in this module, find an expression for the resulting Lorentz force.

(b) Comment on whether this is a good approximation or if a more complicated model should be utilized.

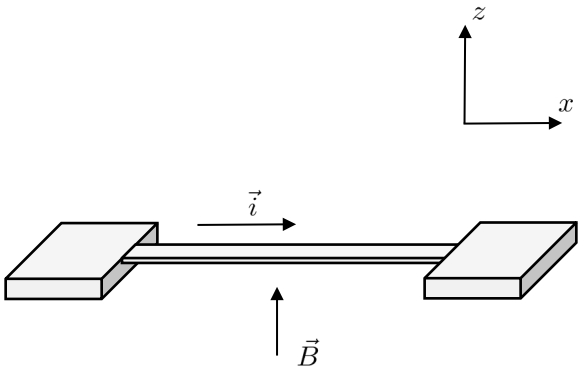

Example 11.3

Given: Consider the magnetomotively-actuated microcantilever shown below.

Find: Find an expression for the resulting Lorentz force.

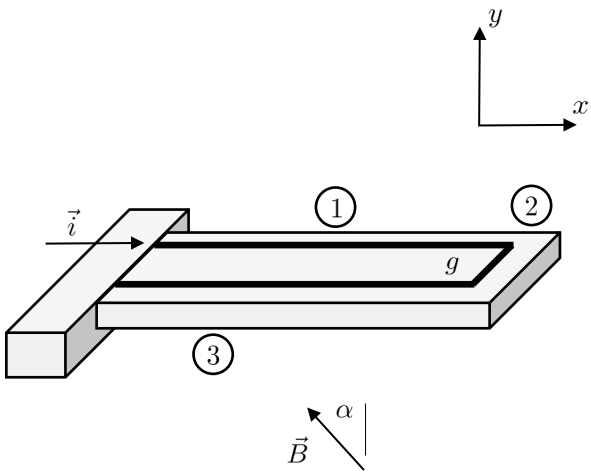

Example 11.4

Given: Consider the magnetomotively-actuated nanowire shown below.

Find: Find an expression for the back EMF produced via motion of the nanowire.

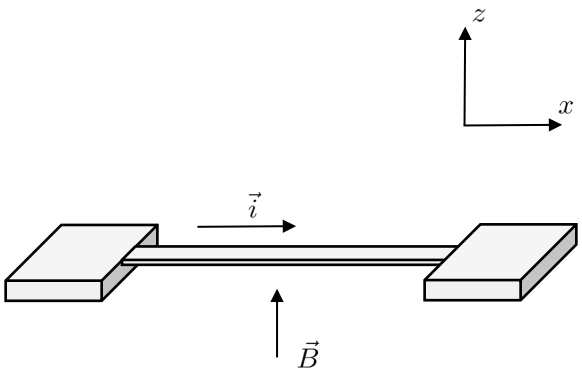

Chapter 12

Thermal Transduction

12.1 Overview

Thermal transducers are pervasive at the micro/nanoscales. As such, rather than attempting to capture the mechanics and heat transfer associated with all of these systems, this module focuses on those transducers which leverage thermal expansion for transduction purposes; specifically, bimorph and chevron actuators.

Thermal expansion refers to the fact that structures tend to expand volumetrically under increasing heat. Mathematically, this expansion can be expressed volumetrically or linearly.

The *volumetric thermal expansion coefficient* γ is defined as:

(12.1)

where ΔV represents the change in volume, V represents the initial volume, and ΔT is the imposed change in temperature. This is often rewritten in terms of the volume change ΔV:

(12.2)

The *linear thermal expansion coefficient* α is defined as:

(12.3)

where ΔL represents the change in length, L represent the initial length, ΔT is the imposed change in temperature, and ε_{xx} specifies the uniaxial strain in the element. This is often rewritten in terms of the length change ΔL:

(12.4)

or temperature-dependent strain:

(12.5)

Note that the volume and linear thermal expansion coefficients are related to one another:

(12.6)

12.2 Thermoelastic Transducers

The thermal expansion mechanism detailed above can be easily exploited for transduction purposes. However, it is not without problems. Consider, example, a thin silicon strip. The thermal expansion coefficient for silicon $\alpha_{SI} = 2.6 \times 10^{-6}$ /K. Thus, if the strip is 1 mm long, it will only extend 0.26 μm with a 100 K rise in temperature. As such, clever mechanisms for mechanical amplification are necessary to fully exploit the thermoelastic effect.

Key Result: Before proceeding with the modeling and analysis of specific transducers, it is prudent to highlight the benefits and drawbacks of thermoelastic transducers:

- Benefits:
  - Large mechanical displacements are possible *with amplification.*
  - Small form factor.
- Drawback:
  - Comparatively-large power consumption metrics, due to a reliance Ohmic heating.
  - Comparatively-low response times, due to a reliance on heat transfer mechanisms (primarily conduction).

12.3 Thermal Bimorph Actuators

Arguably the most common thermoelastic transducer is the *bimorph actuator* which utilizes a composite structure comprising of two materials with dissimilar thermal expansion coefficients to achieve large deflections.

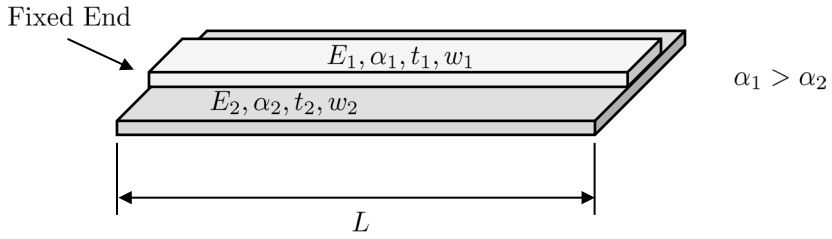

Under an imposed temperature difference ΔT the system deforms as shown.

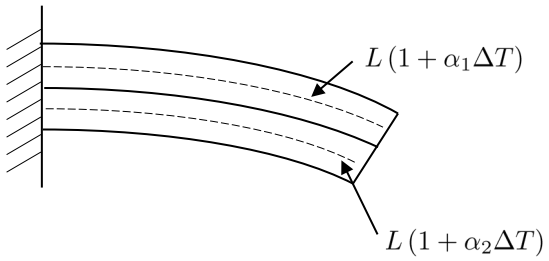

This deformation yields a radius of curvature ρ given by [7]:

$$\frac{1}{\rho} = \frac{6w_1w_2E_1E_2t_1t_2\,(t_1+t_2)\,(\alpha_1-\alpha_2)\,\Delta T}{(w_1E_1t_1)^2 + (w_2E_2t_2)^2 + 2w_1w_2E_1E_2t_1t_2\left(2t_1^2+3t_1t_2+2t_2^2\right)}, \tag{12.7}$$

where E_1, E_2, α_1, and α_2 represent the modulus of elasticity and thermal expansion coefficient of each layer, respectively, and all other parameters are defined as in the figure included above.

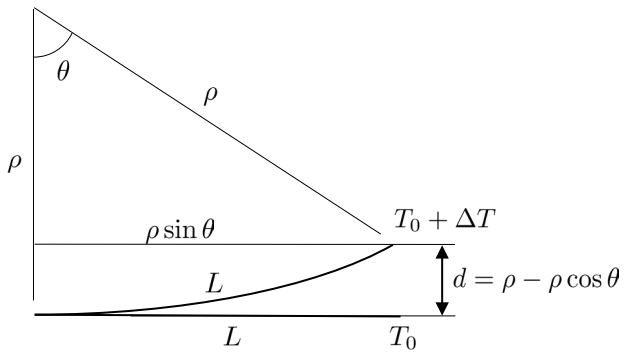

Simple trigonometry yields:

(12.8)

This, in turn, yields a tip deflection given by:

(12.9)

Expanding this in a Taylor Series yields:

(12.10)

12.4 Other Thermoelastic Actuators

To understand the operation of non-bimorph thermoelastic actuators, it proves helpful to first consider the generic system shown below.

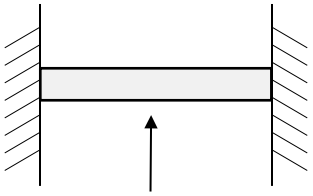

Previously in this module it was shown that

$$\varepsilon_{xx} = \alpha \Delta T, \tag{12.11}$$

where ε_{xx} is the uniaxial strain resulting from an imposed temperature change ΔT assuming the linear thermal expansion coefficient of the material is α.

If the material is constrained such that it is not allowed to expand, then:

(12.12)

where σ_{xx} is the uniaxial stress developed in the structure and E is the material's modulus of elasticity.

Solving this equation for σ_{xx} yields:

(12.13)

The reactive fore generated at the boundaries is thus:

(12.14)

Note that this is commonly quite large.

The energy ΔE required to heat the system of interest such that a temperature change ΔT results is at least:

(12.15)

where c_P, ρ, and V are the heat capacity, mass density, and volume of the material, respectively. This, however, fails to account for energy loss at the system's boundaries.

Examining the generic system detailed above, it can be seen that large forces, but small displacements are achievable with thermoelastic actuation. To increase the practical utility of these systems, the following actuation mechanisms are commonly employed.

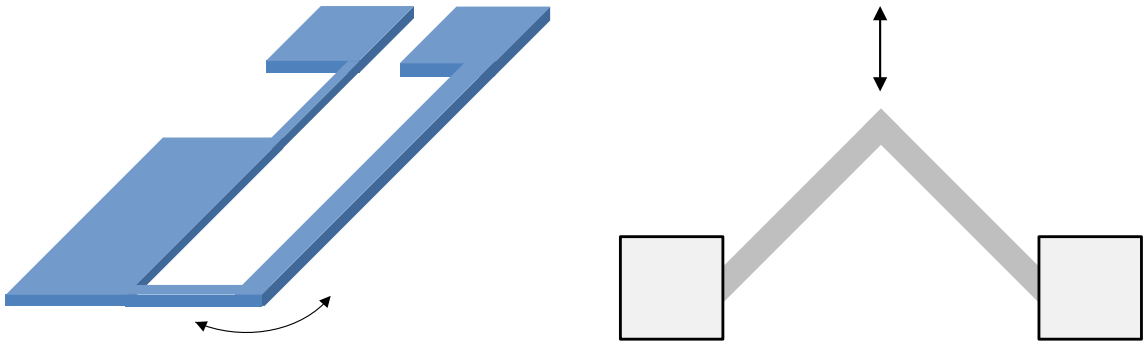

Example 12.1

Given: Consider the bimorph actuator shown below. Assume the structure has width $w = 20$ μm and length $L_{AB} = L_{BC} = 100$ μm; the aluminum layer ($E_{Al} = 70$ GPa, $\alpha_{Al} = 2.5 \times 10^{-6}$ /K) is of thickness $t_{Al} = 0.5$ μm; the silicon nitride layer ($E_{SN} = 250$ GPa, $\alpha_{SN} = 3 \times 10^{-6}$ /K) is of thickness $t_{SN} = 1$ μm; and there is an imposed temperature change of $\Delta T = 20$ K.

Find:
(a) Find the radius of curvature ρ.
(b) Find the displacement at point B δ_B.
(c) Find the displacement at point C δ_C.

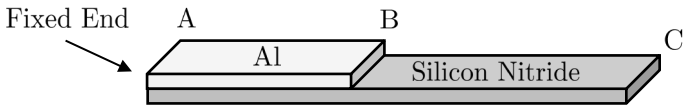

Example 12.2

Given: Consider the silicon chevron actuator shown below. Assume $y_0 = 10$ μm, $L_0 = 200$ μm, and there is an imposed temperature change of $\Delta T = 300$ K.

Find: Find the tip displacement of the actuator Δy.

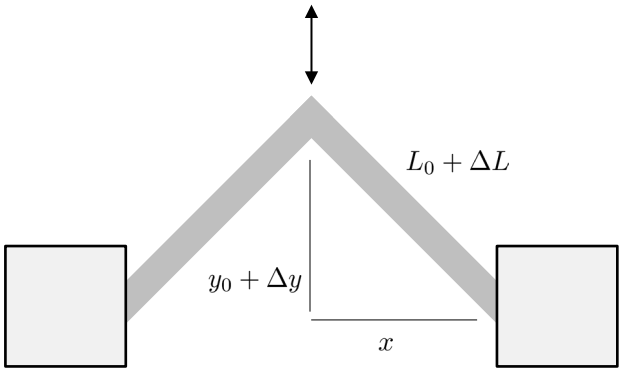

Chapter 13

Near-Field Interactions

13.1 Overview

Thus far, this lecturebook has focused on the modeling and analysis of elastic structures, resonators, and the most common transduction mechanisms utilized in MEMS and NEMS. Despite the emphasis on these key enabling topics, there are a number of additional physical mechanisms that exist at small scales, which often have to be addressed in system design. These include noise, nonlinearity, uncertainty, and near-field interactions, amongst many others. This module focuses on *near-field effects* such as capillary forces, adhesion forces, van der Waals/Casimir forces, and local repulsive forces.

13.2 Near-Field Forces

Though captured by two distinct force models, the *van der Waals* and *Casimir forces* both capture local interactions which take place between close bodies (often separated by nm-scale gaps) and result from quantum mechanical effects.

According to quantum theory, electromagnetic fields fluctuate, and thus they can never be exactly zero. This leads to a finite zero-point energy (fluctuation). As noted in [14], the fact that this zero-point energy density, assumed here to be between two conducting plates, is lower than that of free space, renders an attractive force.

The attractive force between two plates or a plate/sphere combination is typically classified by the distance between geometries. Classic studies involving aluminum and gold plates have indicated that:

- van der Waals models are appropriate for gaps between 0.5 nm and 4 nm.
- Casimir models are appropriate for gaps between 4 nm and 1 μm.
- For gaps greater than 1 μm, the effects are commonly negligible.

13.2.1 Casimir Force

The *Casimir* or *retarded van der Waals force* is typically modeled by:

(13.1)

for plate/plate interactions, and by

(13.2)

for plate/sphere interactions, where $\hbar$ is the reduced Planck constant (divide by 2π), c is the speed of light, g is the instantaneous gap, and R is the radius of the spherical surface.

Note that this force, which scales like l^{-4} for plate/plate interactions commonly has magnitudes ranging from 1 fN - 1 nN over the applicable range of gap.

13.2.2 van der Waals Force

van der Waals force is typically modeled by:

(13.3)

for plate/plate interactions, and by

(13.4)

for plate/sphere interactions, where H represents the Hamaker constant, a material property dependent on the two materials which typically varies between 0.4 - 4 $\times 10^{-19}$ J.

Note that this force, which scales like l^{-3} for plate/plate interactions cmomonly has magnitudes ranging from approximately 1 nN - 1 μN over the applicable range of gap.

While the practical value of Casimir forces is still to be determined, a number of works have identified the impact of the force, as well as van der Waals force, on stiction, pull-in, and adhesion. Another domain/application space which relies on these forces is atomic force microscopy. Given the breadth of study necessary to fully characterize that topic, further discussion is omitted here.

13.3 The Lennard-Jones Potential

Thought the models detailed above are useful for describing the static and dynamic behavior of MEMS and NEMS which stay within a given force regime, they fail to capture the strong repulsion that must exist between surfaces which are extremely close (due to the issue of overlapping electron orbitals) or transitions across forcing regimes. One model which does capture these behaviors, at least phenomonologically, is the *Lennard-Jones potential*.

The Lennard-Jones potential is typically expressed as:

(13.5)

which yields a force of the form:

(13.6)

where A, B, $\bar{A}$, $\bar{B}$ are constants which depend on both system geometry and material. If the interaction area is sufficiently small, these expressions are often rewritten under the assumption of a sphere/plate interaction model:

(13.7)

(13.8)

where A_1 and A_2 are functions of the Hamaker constant, and R is the radius of the sphere.

Each of the force models presented in this module can be appended to the previously-developed system models as necessary to account for near-field interactions.

Chapter 14

Noise in MEMS and NEMS

14.1 Overview

From the field of physics, it is well known that the thermal noise energy of a system is $k_B T$, where k_B is Boltzmann's constant and T is the system's instantaneous temperature. From a scaling perspective, it is clear that this energy is length scale independent. In contrast, it is known that signal amplitudes (and thus power) typically decrease with length scale. This competition between a length-dependent effect and the length-independence of thermal noise makes the topic of noise critical to the predictive design of MEMS and NEMS. Please note that further discussion of the topics described within this module can be found in [10].

In a very generic sense, noise is a random fluctuation of electrons and atoms. For example, the random motion of electrons leads to voltage noise and the random thermal vibrations of atoms leads to mechanical displacement noise. For the sake of instruction, the present module begins with a discussion of electrical noise and then extends the results to mechanical and electromechanical systems.

Generally speaking, it is impossible to predict the magnitude, frequency, and phase of a measured signal. As such, these signals must be characterized statistically. One way this is commonly done is by looking at probability distributions. The majority of physical noise sources are governed by a Gaussian Distribution:

(14.1)

where, for example, V_n is the measured voltage and V_{rms} is the root-mean-squared (RMS) voltage or standard deviation from the average voltage.

The probability a measured voltage V_n is between the values of V_1 and V_2 is:

(14.2)

Due to the shape of the distribution:

- The probability of noise being within V_{rms} of the mean is 68%.
- The probability of measure noise voltages over $3V_{rms}$ is $\leq 0.3\%$.

Note that V_{rms} can also be calculated using classical root-mean-square techniques, that is:

$$V_{rms} = \lim_{N \to \infty} \sqrt{\frac{1}{N} \sum_{n=1}^{N} V_n^2} \tag{14.3}$$

If multiple uncorrelated noise sources are present, the net V_{rms} can be found from:

(14.4)

where p is the number of sources.

If multiple correlated noise sources are present, the net V_{rms} can be found from:

(14.5)

14.2 Noise in the Frequency Domain

RMS noise V_{rms} effectively characterizes noise in the time domain, but fails to identify frequency information. When this information is important, the power spectral density $\overline{V_n^2}$ and spectral density $\overline{V_n} = \sqrt{\overline{V_n^2}}$, which define how much noise exists per unit bandwidth at a given frequency, are used.

Note,

(14.6)

14.2.1 White Noise

White noise is a frequency-independent noise with constant spectral density. That is, $\overline{V_n}(f) = \overline{V_n}$.

Since real systems have finite bandwidth, the noise is commonly expressed in conjunction with a transfer function $H(f)$:

(14.7)

where

(14.8)

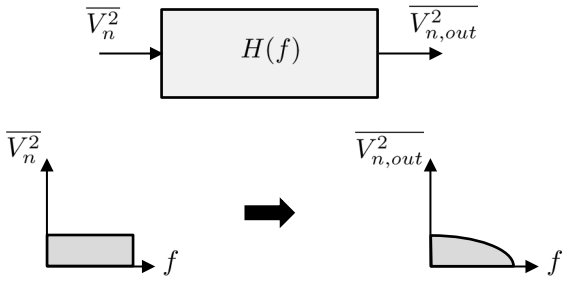

The V_{rms} output noise associated with a white-noise excited system is given by:

(14.9)

The noise bandwidth associated with the system is given by:

(14.10)

where H_{pk} is the peak value of the transfer function. This yields:

(14.11)

14.2.2 Flicker Noise ($1/f$ Noise)

Flicker noise is endemic to many electrical and mechanical systems. In electrical systems it is commonly attributable to the random behaviors of electrical carriers (trapping, release, etc.). In mechanical systems it can be related to some sources of nonlinearity and surface effects.

At the microscale, electrical $1/f$ noise typically dominates. However, at the nanoscale, the important of $1/f$ mechanical noise is still being determined.

The spectral density of flicker noise $\overline{V_{1/f}}$ can be expressed as:

(14.12)

where f_c is the $1/f$ corner frequency, or more specifically, the frequency where the power spectral density of the $1/f$ noise and the white noise $\overline{V_n^2}$ have equal amplitude.

Combining some of the previous results developed in this module, renders the useful relationship:

(14.13)

Note that ideally to evaluate the above expression, the integration should be performed over the entire frequency interval, but doing so yields infinite noise. Fortunately, this would also require and infinitely-long measurement and thus is of minimal concern.

14.3 The Equipartition Theorem

From thermodynamics, and more specifically the *Equipartition Theorem*, it is known that the average thermal energy for each *degree of freedom* in a system is:

(14.14)

where k_B is Boltzmann's constant and T is the instantaneous temperature of the system.

In mechanical systems such as simple harmonic resonators, there are typically two degrees of freedom per system: velocity and position. Thermal noise in these systems typically takes the form of Brownian motion.

In electrical systems the number of degrees of freedom is typically the total number of independent inductors and independent capacitors (i.e. inductors which are not coupled directly in series with another inductor or capacitor, and capacitors which are not coupled directly in parallel with another inductor or capacitor). Thermal noise in these systems typically takes the form of Johnson-Nyquist noise.

14.4 Thermal Noise in Electrical Systems

The average thermal energy in a capacitor is given by:

(14.15)

The stored energy in the same capacitor due to a voltage is

(14.16)

where C defines the system's capacitance and V_{rms} is the associated RMS voltage. Equating these expressions yields:

(14.17)

Accordingly, the thermal noise in the capacitor only varies with C and T.

Similarly, the average energy stored in an inductor is:

(14.18)

where, L defines the system's inductance and i_{rms} is the associated RMS current. Equating as before yields:

(14.19)

Accordingly, the thermal noise in the inductor only varies with L and T.

The frequency spectrum of this noise depends on the amount of resistance in the system:

(14.20)

Alternatively:

(14.21)

14.5 Thermal Noise in Mechanical Systems

Consider the mass-spring-dashpot system shown below.

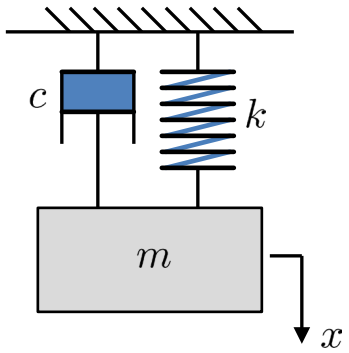

Mimicking the procedure previously adopted for electrical systems, it can be shown that:

(14.22)

where W_{kin} is the average kinetic energy stored in the system, $\dot{x}_{rms}$ is the RMS velocity, and all other parameters are defined as shown. This yields:

(14.23)

Likewise, it can be shown that:

(14.24)

where W_{pot} is the average potential energy stored in the system and x_{rms} is the RMS position. This yields:

(14.25)

Apart from these expressions, it is sometimes useful to express a noise force generator which is analogous to a frequency-dependent voltage:

(14.26)

the use of this and the other expressions developed thus far will be illustrated via example.

14.6 Signal to Noise Ratio

The signal to noise ratio (SNR) of a system is defined according to:

(14.27)

where P_S is the power of the signal of interest and P_N is the power of the noise in the system. In electrical systems:

(14.28)

and

(14.29)

Thus

(14.30)

In dB units:

(14.31)

The key takeaway from this is that, in an absolute sense, noise amplitude is irrelevant and only SNR matters.

14.7 A Brief Note on Averaging

The common methods of reducing the impact of noise rely on signal averaging, or the averaging of multiple signal measurements.

Consider for example, measurements made in the presence of white noise. Since these measurements are uncorrelated, the average RMS voltage $< V_{rms} >$ can be expressed as

(14.32)

where $V_{rms,i}$ is the RMS voltage of the ith measurement and N is the total number of measurements made.

If the signal stays constant during measurement, the average signal $< V_S >$ is defined according to

(14.33)

where $V_{S,i}$ is the voltage associated with the ith measurement. Accordingly, the signal to noise ratio associated with the system is:

(14.34)

As such, averaging helps the SNR, though, in the case of this example, this result is based on a constant signal assumption, which is bandwidth limited.

In contrast, in the case of $1/f$ noise the measurements are correlated, thus

(14.35)

Likewise, if the signal is constant:

(14.36)

Therefore,

(14.37)

Accordingly, averaging does not help.

Example 14.1

Given: Consider the noise in a piezoresistive sensor. Assume the sensor has an associated thermal noise density $\overline{V_n} = 2$ nV/$\sqrt{\text{Hz}}$ and corner frequency $f_c = 4$kHz.

Find: Find the total sensor noise from 0.1 Hz to 10 kHz.

Example 14.2

Given: Consider the behavior of a Silicon bead suspended in liquid. Assume that a velocity-proportional friction force acts on the bead, the system is at a nominal temperature T, and that the bead has mass density ρ and is of radius R.

Find: Find the RMS velocity $\dot{x}_{rms}$ of the system as a function of the bead radius R.

Example 14.3

Given: Reconsider the previous example, but now assume that the dominant external force derives from a tether which has a spring stiffness k which scales with mass such that the frequency of the system $f_0 = 1$ kHz = constant. As before, assume that the system is at a nominal temperature T, and that the bead has mass density ρ and is of radius R.

Find: Find the RMS displacement x_{rms} of the system as a function of the bead radius R.

Chapter 15

Fluidic Dissipation in MEMS and NEMS

15.1 Overview

Unlike noise and near-field effects, which often limit the performance of micro- and nanosystems near the *bottom end* of their performance range, dissipation and nonlinearity often constraint performance on the *upper end* where large and fast motions are desired. This module focuses on dissipation, leaving discussions of nonlinearity to subsequent modules.

Energy dissipation in micro/nanosystems arises from a wide variety of effects, including:

- Fluid Damping (Drag, squeeze-film, etc.)
- Anchor Losses
- Thermoelastic Effects
- Surface Losses
- Phonon/Phonon Interactions
- Phonon/Electron Interactions

This module addresses the first form of damping on this list, leaving the others for future consideration.

15.2 Damping Coefficients and Quality Factors

In general, scientists and engineers are concerned with damping in second-order systems, which may or may not be resonators:

$$m\ddot{x} + c\dot{x} + kx = F(t). \tag{15.1}$$

Here, m, c and k define the system's effective mass, damping, and stiffness, x is a local displacement variable, and $F(t)$ is an applied force. As previously demonstrated, this equation of motion is commonly rewritten as:

(15.2)

or

(15.3)

where ω_n, ζ, and Q are the natural frequency, damping ratio, and quality factor associated with the system, respectively, and $f(t)$ is the mass-normalized applied force.

Implicit in this model is that the dissipative force $F_d = -c\dot{x}$ is velocity proportional and the quality factor Q is defined according to:

(15.4)

Note that if damping arises from multiple sources:

$$c_{total} = \sum_{i=1}^{N} c_i. \tag{15.5}$$

Thus,

$$\frac{1}{Q_{total}} = \sum_{i=1}^{N} \frac{1}{Q_i}. \tag{15.6}$$

In general, Qs will range from ≈1, for devices in liquid, to ≈10-500 for devices in air, to $> 10,000$ for devices in vacuum.

To a certain extent, packaging can be used to control fluid damping. Other, so-called intrinsic forms of damping are very difficult to control at room temperature.

15.3 Fluid Damping

In most micro/nanosystems, fluid damping is the dominant mechanism of energy dissipation.

In situations where the device of interest is well isolated and operating at atmospheric pressure and room temperature, primitive fluid drag models are occasionally used. In these models,

(15.7)

where ρ is the density of the fluid, C_D is a geometry-dependent drag coefficient, A is the projected area of the structure, and n is a velocity power that is dependent on the system's Reynolds Number.

The Reynolds number Re associated with a fluid-structure interaction is defined according to:

(15.8)

where ν is the kinematic viscosity of the fluid (a material property), $v = |\dot{x}|$ is the speed of the structure, and L is a characteristic length associated with the system. If $Re < 1000$, then $n \approx 1$.

Likewise, if $Re > 1000$, the $n \approx 2$.

Note that while this model does a fairly good job of estimating dissipation in macroscale systems, it has largely been neglected, as or late, at smaller scales due the emergence of refined models.

15.4 Air Damping and the Knudsen Number

At pressures close to atmospheric, air viscosity is independent of pressure. In this damping regime, the so-called *viscous regime*, air acts as a viscous fluid and the damping coefficient is independent of pressure.

As pressure is reduced the damping mechanisms start to transition from a viscous regime to a *molecular regime*. This transition is governed by the mean free path λ of the surrounding medium, that is, the distance an air molecule can travel before impacting another molecule.

At atmospheric pressure, $\lambda = 65$ nm. However, as pressure is decrease, the mean free path increases until it becomes on the same order as a characteristic device dimension d_c. At this point damping is in the *molecular regime*, wherein molecular interactions dominate dissipation.

Further decreasing pressure levels from this point, leads to an *intrinsic regime*, wherein fluid dissipation is insignificant and material effects dominate.

The mean free path of a gas λ is defined as

(15.9)

where d_g is the effective diameter of the gas molecule and n_V is the number of gas molecules per unit volume.

The Ideal Gas Law states:

(15.10)

where $N_A = 6.022 \times 10^{23}$ /mol is Avogardo's Number, $R = 8.3145$ J/mol K is the Universal Gas Constant, and T is the gas temperature. Combining these results yields:

(15.11)

The Knudsen Number Kn is defined according to:

(15.12)

where d_c is the characteristic device length, which is typically selected to be the smallest length dimension in the system.

- If $Kn < 0.1$, damping is in the *viscous regime* and continuum models are valid.
- If $0.1 < Kn < 10$, damping is in the *transition regime* and modified continuum models are needed.
- If $Kn > 10$, damping is in the *molecular regime* and continuum models are invalid.

15.5 Beams Isolated from a Substrate

Fluid dissipation models for MEMS and NEMS are still very much in a development and validation stage of research. However, one common, well-understood scenario in the MEMS/NEMS community is the force exerted on a cantilevered beam well isolated from a substrate.

The dissipation associated with a cantilevered beam moving through a viscous fluid is typically modeled by a formula popularized by Sader in 1998 [15]. Here,

(15.13)

where μ is the mass per unit length of the beam, ρ is the density of the substance, b is the nominal width of the structure, $\Gamma_r(\omega_R)$ and $\Gamma_i(\omega_R)$ are the real and imaginary parts of the associated hydrodynamic function, and ω_R is the natural frequency of the structure in the absence of a dissipative mechanism.

The hydrodynamic function $\Gamma(\omega_R)$ can be recovered from the geometry and Reynolds number associated with the system:

(15.14)

(15.15)

where Re_b is the Reynolds number associated with the characteristic length b and Ω is a polynomial fit function and K_0 and K_1 are modified Bessel functions of the 3rd kind. Readers interested in applying this model to a particular system are encouraged to read [15] or [16].

Within the molecular regime, a quality factor model popularized by Blom in 1992 is commonly employed [17]:

(15.16)

where

(15.17)

Here, M is the mass of a given gas molecule, R is the gas constant, T is the gas temperature, d is the thickness of the beam, l is the length of the beam, ρ_s is the density of the solid, and E is the elastic modulus of the solid.

Recently, Bidkar, et al. proposed a unified theory [18].

15.6 Fluid Dissipation Near a Substrate

Thus far, this module has focused on damping models which are appropriate when the device of interest is well isolated from its substrate. However, in most MEMS/NEMS devices a substrate is present and capable of influencing the system's behavior. Accordingly two additional fluidic dissipation mechanisms must be considered:

- *Squeeze-film damping*, wherein the device moves closer to the substrate perpendicularly; and
- *Lateral damping*, wherein the device moves parallel to the substrate.

A model for lateral damping is considered first here, since it is fairly well accepted by the research community. Squeeze-film damping will be considered second, since models for this phenomenon are a source of contention within the community.

15.6.1 Lateral Damping

In scenarios such as that shown below, where the device's motion is parallel to the substrate, the principal source of fluid dissipation is shear flow.

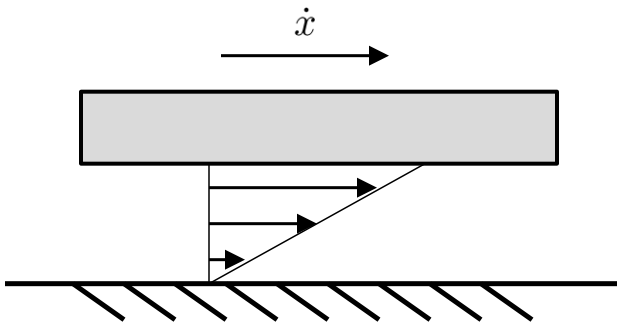

In this scenario, the damping coefficient c is given by

(15.18)

where A is the total plate area, d is the gap between device and substrate, and μ_{eff} is the effective viscosity defined to be

(15.19)

where μ is the traditional viscosity and Kn is the Knudsen number associated with the system.

15.6.2 Squeeze-Film Damping

Consider the case of a rigid plate approaching a substrate, as shown below.

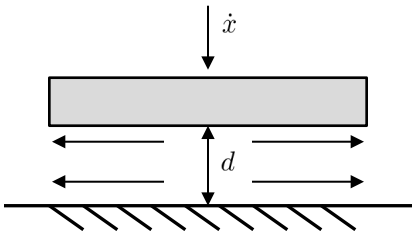

- If the approach is comparatively slow, the air is *squeezed* out and energy is lost.
- If the approach is comparatively fast, the air also yields an effective spring force.
- If the approach is comparatively fast and periodic, the air also yields an additional effective mass.

In large Knudsen number situations, this form of damping is modeled with the assistance of an effective viscosity:

(15.20)

where μ is the viscosity under normal conditions (i.e. $Kn << 0.1$) and Kn is the Knudsen number associated with the system. Please note that as $Kn \to 0$, $\mu_{eff} \to \mu$. This effective viscosity can be exploited to derive:

(15.21)

(15.22)

where m and n are odd integers, p is the fluid pressure, $\alpha = w/l$ is the width to length ratio (assuming $w << l$), $\sigma = 12\mu_{eff}w^2\omega/pd^2$ is the so-called squeeze number, d is the thickness of the plate, and ω is the frequency of oscillation. Note that this model assumes Re is small and the added-mass effect is negligible.

As noted in [10], if $\sigma/\pi^2 << 1$ and $\alpha = 1$ (i.e. the plate is square), then

$$c = 0.42\frac{\mu_{eff}A^2}{d^3}, \tag{15.23}$$

$$k_{air} = 0.25\frac{\mu_{eff}^2 A^3\omega^2}{pd^5}. \tag{15.24}$$

The two graphs provided below detail the pressure-dependent characteristics of squeeze-film damping. Remember that in practice these need to be carefully constructed and analyzed, as there is both a direct and indirect dependence on pressure [e.g. $\mu_{eff}(Kn) \rightarrow Kn(\lambda) \rightarrow \lambda(p)$, thus $\mu_{eff}(p)$].

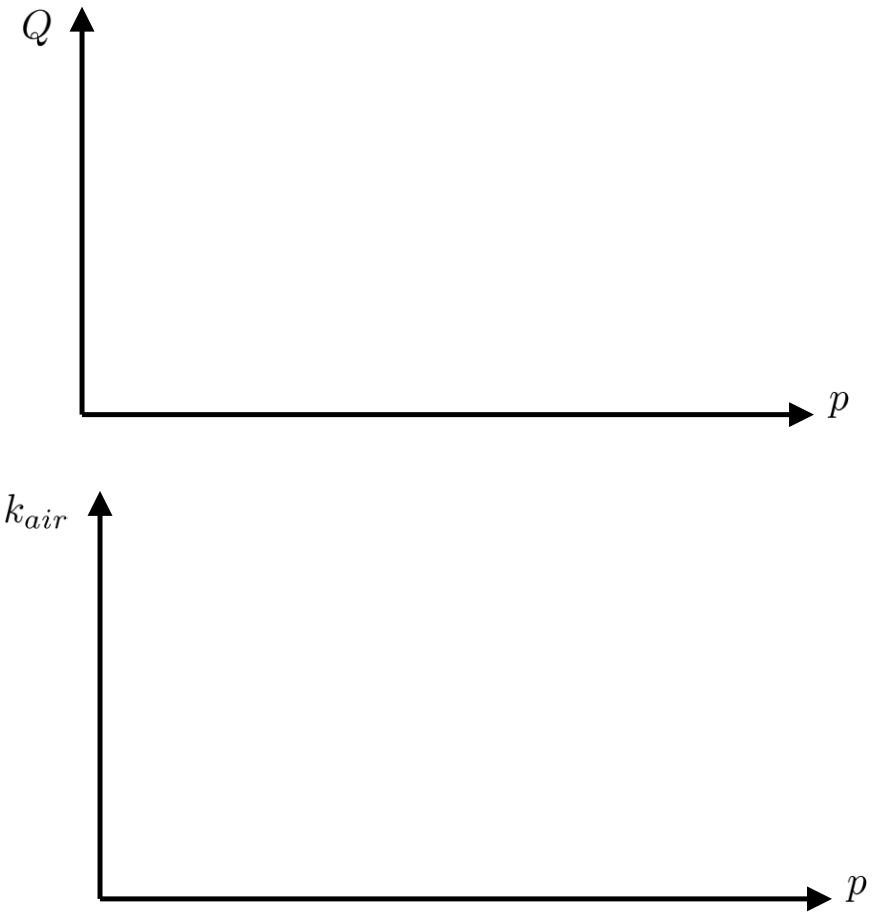

15.6.3 Mitigating the Squeeze-Film Effect

To partially mitigate the squeeze-film effect, many researcher have moved towards device perforation. This often does not require further processing during fabrication, due to the common addition of etchant paths on devices with a significant surface area.

In these systems,

(15.25)

where r_c is the cell radius, $A = N\pi r_c^2$ is the plate area with N holes, $\beta = r_o/r_c$, r_o is the hole radius and $K(\beta) = 4\beta^2 - \beta^4 - 4\ln\beta - 3$. Note that this model does not account for the flow resistance associated with the holes.

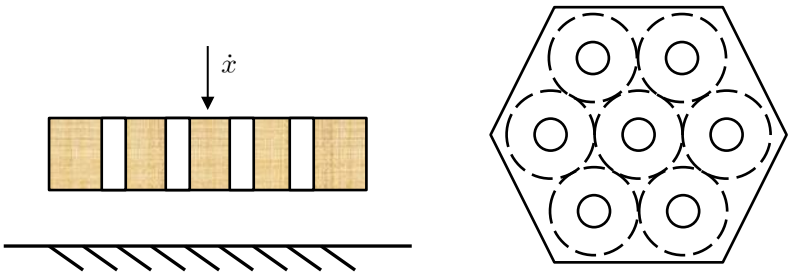

Side View Top View

Chapter 16

Other Dissipation in MEMS and NEMS

The previous module considered the effects of fluidic dissipation, the dominate source of energy loss in micro/nanoscale devices. The present module picks up from this point, briefly describing some of the *intrinsic* forms of dissipation that can exist in small-scale systems.

16.1 Anchor Loss

Despite the fact that the boundary conditions of vibrating beams and plates are typically modeled as if they were rigid, in reality, there is a measurable energy loss attributable to the finite deformation of supports.

The amount of energy lost at a given support is dependent on the mode shape of oscillation and the type of support utilized. Given the complexity of the required structural analysis, Q is commonly estimated from an infinite elastic anchor approximation for a cantilevered beam. This yields:

(16.1)

where L and t are the length and thickness of the beam, respectively.

While the aforementioned formula does a decent job approximating anchor loss for cantilevered systems, it is important to get a qualitative feel for this mechanisms and its relevance to design.

Beams with fixed-fixed boundary conditions typically have high anchor losses due to the need for beam and support deformation.

Tuning fork structures tend to have minimal anchor loss due to an approximate cancelation of stress fields in the support.

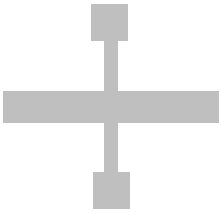

Longitudinal-mode devices typically have little anchor loss because the supports are placed at nodes (points of zero or near-zero displacement).

16.2 Thermoelastic Dissipation

Another source of dissipation in micro/nanosystems is associated with the periodic heating of devices due to an induced strain. More specifically, this dissipation arises from the fact that conduction within a vibrating device typically occurs on time scales which are much faster than those associated with conduction and convection to the environment. As such, the surfaces of the structure are nominally adiabatic and heat flows across the thickness of the structure, in a periodic manner, from the hot side (in compression) to the cool side (in tension).

This bulk thermoelastic effect can be modeled for a cantilevered beam as:

(16.2)

where $\Gamma(T)$ captures the temperature-dependent behavior attributed to material properties and $\Omega(f)$ relates the mechanical motion to a reference state. $\Gamma(T)$ is defined as:

(16.3)

where α, E, ρ, and c_p are the coefficient of thermal expansion, modulus of elasticity, mass density, and specific heat associated with the device, respectively, and T is the temperature of the device. $\Omega(f)$ is defined as:

(16.4)

where f is the cantilever oscillation frequency, κ is the thermal conductivity associated with the device, and

(16.5)

is a characteristics frequency associated with the device. Note that this model assumes that the device is fabricated from an isotropic, homogeneous material. In polycrystalline materials, the situation is appreciably more complex to the presence of both intracrystalline and intercrystalline thermoelastic dissipation [19].

16.3 Surface Losses

Though few, if any, experimentally-validated models for surface losses exist, it is clear that Q decreases with an increased surface to volume ratio. In an intrinsic scenario, this has been attributed to:

- Surface stress;
- Adsorption/absorbtion;
- Interactions between surface waves and acoustic waves; and
- Surface rearrangement.

16.4 Phonon/Phonon Interactions

As noted in [20], dissipation can also arise to anharmonicity in a given crystal lattice and the interaction between thermal phonons and acoustic modes of vibration. This can be attributed to the fact that the *sound* waves can perturb the phonons away from equilibrium, and the return to equilibrium is a dissipative process.

The Q associated with this intrinsic process is given by:

(16.6)

where ν is the sound velocity in the material, $\hat{\gamma}$ is Grueisen's Constant (which characterizes the anharmonicity of the lattice), c is the heat capacity of the material per unit volume, ω is the frequency of motion, and τ_{ph} is the phonon relaxation time given by:

(16.7)

where κ and ν_D are the thermal conductivity and Debye sound velocity of the material. Note that the Debye sound velocity is defined to be

(16.8)

where ν_l and ν_t are the velocities of longitudinal and transverse sound waves in the material.

16.5 Phonon/Electron Interactions

In metals and potentially some semiconductors, dissipation due to phonon/electron interactions is also possible. The concept here is that strain leads to ion oscillations, and free electron transport. To some extent, this electron flow has an associated viscosity and the interaction of this flow with sound waves is dissipative in nature.

The Q associated with this dissipative process is given by:

(16.9)

where m_e is the electron mass, e is the electron charge, σ is the electrical conductivity of the material, $\mathcal{E}_F$ if the Fermi energy associated with the system, and all other parameters are defined as before. Additional details on this dissipation mechanism can be found in [20].

Chapter 17

Nonlinearities in MEMS and NEMS

17.1 Sources of Nonlinearity in MEMS and NEMS

If one considers the entirety of systems in the universe, as well as the universe itself, linear systems make up just a very small subset of the total set of systems. Furthermore, this linear subset itself exists on a foundation of simplifying assumptions. Because of this, practicing scientists and engineers must familiarize themselves with nonlinearities and associated response phenomena. This is particularly true in the case of MEMS and NEMS, as these small-scale systems have the propensity to demonstrate a wide array of nonlinear behaviors due to their inherently limited dynamic range.

Strictly speaking, a *nonlinear system* is any system which is not linear!

The list below provides a brief overview of system of the sources of nonlinearities in MEMS and NEMS. Though the list is long, it is by no means comprehensive.

- Large mechanical deformations – for example, hard/soft spring systems, where the elastic restoring force F_s can be expressed as

$$F_s = k_1 x + k_3 x^3 + ..., \tag{17.1}$$

  where k_i, $i = 1, 2, ...$ are the linear and nonlinear spring constants associated with the spring and x is a local displacement variable.

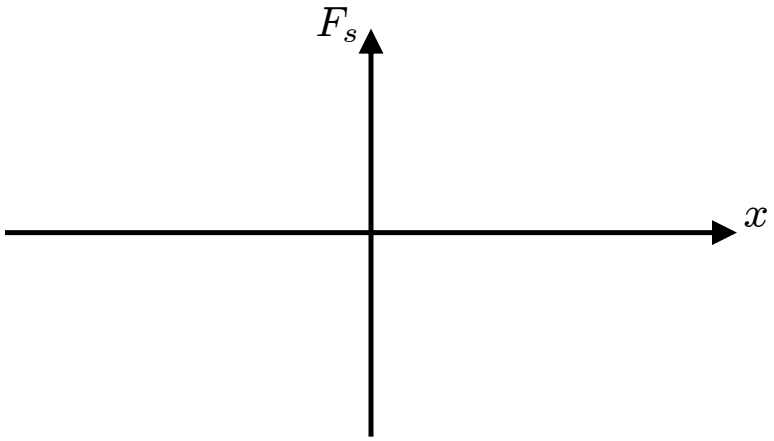

- Transduction mechanisms – for example, variable gap actuators, where the electrostatic actuation force F_{es} can be expressed as

$$F_{es} = \frac{\varepsilon A V^2}{2(g-x)^2} \approx \frac{\varepsilon A V^2}{2g^2}\left(1 + 2\frac{x}{g} + 3\frac{x^2}{g^2} + ...\right), \tag{17.2}$$

  where ε is the permittivity of the gap medium, A represents the electrode area, V is the voltage difference between plates, g is the nominal gap width, and x is a local displacement variable.

- Inertial effects – for example, inertial effects arising in microcantilevers undergoing rapid vibration, where the nonlinear inertial contribution F_I can be expressed as

$$F_I = \alpha \left(\dot{x}^2 x + x^2 \ddot{x} \right) + ..., \tag{17.3}$$

  where α is a geometry- and material property dependent parameter and x is a local displacement variable.

- Material effects – for example, piezoelectric effects, where the material nonlinear contribution F_M can be expressed as

$$F_M = k_2 x^2 + k_3 x^3 + ..., \tag{17.4}$$

  where k_i, $i = 2, 3, ...$ are nonlinear material coefficients which are geometry- and material property dependent.

- Dissipative effects – for example, squeeze-film damping which has a nonlinear contribution that was previously ignored.

- Electrical effects – for example, relay-like behaviors.

- Near-field effects – for example, van der Waals and Casimir forces.

- Contact effects – for example, stiction and other forms of adhesion.

17.2 Nonlinearities in Static/Quasistatic Systems

Consider a generic system model given by:

$$m\ddot{x} + c\dot{x} + kx + f_{nl}(x) = F(t), \tag{17.5}$$

where m, c, and k are the system's effective mass, damping, and stiffness, x is a local displacement variable, $F(t)$ is an applied force acting on the system, and $f_{nl}(x)$ is a nonlinear force acting on the system.

If *static* or *quasistatic* behaviors are of interest, this model reduces to:

(17.6)

The behavior of this system can be analyzed by solving for the local displacement variable x and then characterizing the stability of the system.

Key Result: The quasistatic behavior of an parallel-plate, electrostatic actuator is governed by:

(17.7)

where k represents the actuator's stiffness, γ is a medium- and geometry-dependent constant, g is the initial gap between electrodes, V_{DC} is an applied actuation voltage, and x is a local displacement variable.

This equation can be re-written as:

(17.8)

For the illustration purposes, assume $k = g = \gamma = 1$, this yields:

(17.9)

This equation can be solved to recover $x(V_{DC})$. Plotting this quantity renders the figure shown below. Clearly, multiple steady-state solutions exist, the question is which of these solutions are physically-realizable and stable?

To determine this, consider the force gradients in the vicinity of each solution.

Let

(17.10)

then the associated force gradient can be expressed as:

(17.11)

Note that:

- If

$$\left.\frac{\partial G}{\partial x}\right|_{x=x_0} < 0: \qquad \text{The solution is stable} \tag{17.12}$$

- If

$$\left.\frac{\partial G}{\partial x}\right|_{x=x_0} > 0: \qquad \text{The solution is unstable} \tag{17.13}$$

Leveraging the above relationships renders the stabilities shown above.

17.3 Flow on a Line

Dynamical system are commonly expressed in the state-space form:

(17.14)

where $\mathbf{f}(\mathbf{x}, \mathbf{t})$ is a vector of smooth, real-valued functions. If equation is scalar in form, it is said to be representative of a *first-order system*. Likewise, if $\mathbf{f}(\mathbf{x}, \mathbf{t}) = \mathbf{f}(\mathbf{x})$ it is said to be an *autonomous system*.

The behavior of first-order systems are often characterized through visualizations of the systems; vector fields (i.e. graphs of $\dot{x}$ plotted against x).

Key Result: Consider the vector field

$$\dot{x} = \sin x, \tag{17.15}$$

which is plotted below.

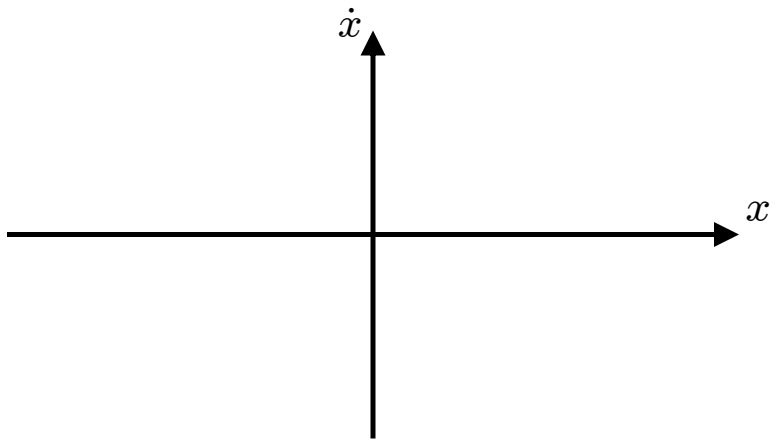

The points where $\dot{x} = 0$ are referred to as *fixed points* or *equilibrium points*. If the flow moves toward the fixed point, the fixed point is considered *stable*. It the flow moves away from the fixed point, the fixed points is classified as *unstable*. With this knowledge in hand, it is relatively easy to sketch a qualitative time response for the system.

While a graphical solution approach often facilitates interpretation, it is often desirable to characterize the nature of a system's response using non-graphical methods. For this, a process of *linearization* is typically adopted.

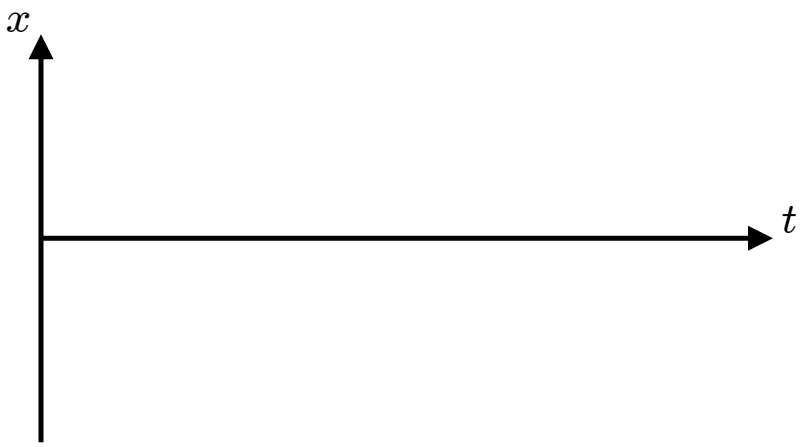

Let x^* be a fixed point of a system and let $\eta(t) = x(t) - x^*$ be a small perturbation of the response. Then,

(17.16)

which yields:

(17.17)

Expanding this results via a Taylor series expansion renders:

(17.18)

If $f'(x^*) \neq 0$ this yields:

(17.19)

Note that:

- If

$$f'(x^*) > 0 \rightarrow \eta(t) \text{ Grows:} \qquad \text{The solution is unstable} \tag{17.20}$$

- If

$$f'(x^*) < 0 \rightarrow \eta(t) \text{ Decays:} \qquad \text{The solution is stable} \tag{17.21}$$

17.4 Linear Systems and Phase Portraits

Two-dimensional, autonomous linear system are often expressed as:

(17.22)

which can be re-written in matrix form as:

(17.23)

where

(17.24)

These higher-dimension system can also be analyzed using graphical and mathematical mechanisms.

Key Result: Consider the mass-spring system shown below. As previously considered, the equation of motion for this system can be expressed as:

(17.25)

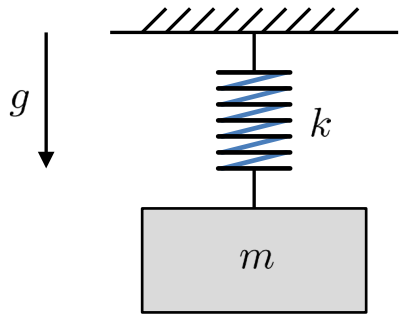

Rewriting this in state-space form yields:

(17.26)

and thus the system's vector field is given by:

(17.27)

This vector field is plotted below.

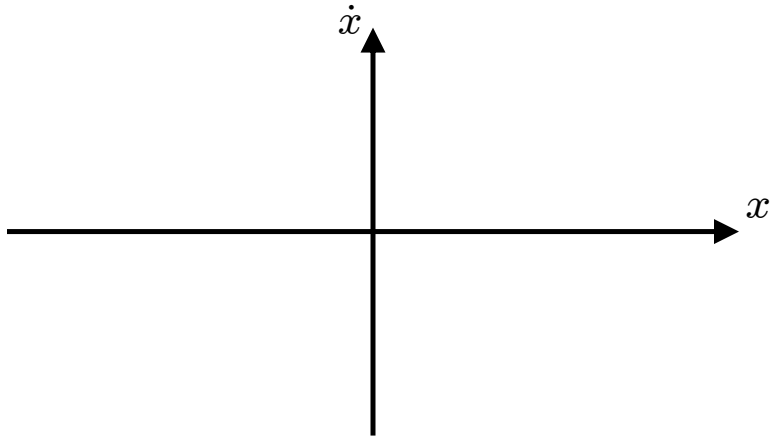

Key Result: Consider the system governed by

(17.28)

Since this system is uncoupled, the system can be *broken down* into a composite of two, first-order systems:

(17.29)

which can be explicitly solved, yielding:

(17.30)

The only fixed point that exists for this system is $(x^*, y^*) = (0, 0)$. The stability of this fixed point changes dramatically with the value of the parameter a as shown below.

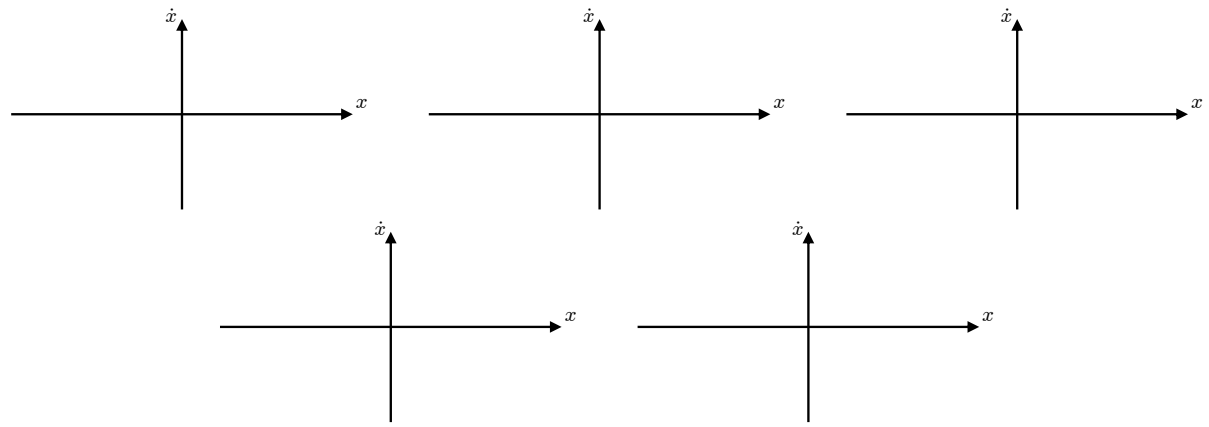

It can be shown that the behavior detailed in the two motivating examples provided above is based on the eigenvalues and eigenvectors of the coefficient matrix $\mathbf{A}$. For a 2×2 matrix these can be expressed in terms of the matrix's trace τ and determinant Δ:

(17.31)

Compiling the results presented here, as well as others, allows for the reconstruction of the graph shown below. As evident, the qualitative nature of the response can change dramatically with parameter variations.

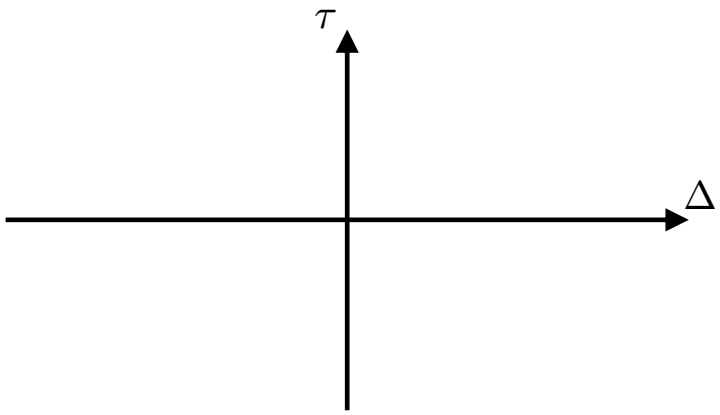

17.5 Nonlinear Systems with Forcing

Thus far, this module has focused on the analysis of static/quasistatic nonlinear behaviors, as well as the behavior of autonomous systems up to second-order (albeit very briefly). The last class of nonlinear problems which commonly arise in the field of MEMS and NEMS are those which involve non-autonomous systems, such as the protypical example presented earlier in the module:

$$m\ddot{x} + c\dot{x} + kx + f_{nl}(x) = F(t). \tag{17.32}$$

The most commonly examined system of this type if governed by the so-called *Duffing equation*:

$$m\ddot{x} + c\dot{x} + k_1 x + k_3 x^3 = f \sin \omega t. \tag{17.33}$$

This system is the simplest system that exhibits *bistability* and *hysteresis* in its frequency response. The solution of this system is commonly expressed as

$$x(t) = X \sin(\omega t + \phi), \tag{17.34}$$

where X and ϕ vary slowly with time and can be multi-valued. The slowly-varying amplitude and phase variables X and ϕ are plotted below as functions of the excitation frequency ω, assuming $k_3 > 0$. Note that if $k_3 < 0$, the response characteristic is flipped. By manipulating the sign and magnitude of this nonlinear coefficient, one can alter the qualitative nature of the response and affect key performance metrics, such as power handling and phase noise.

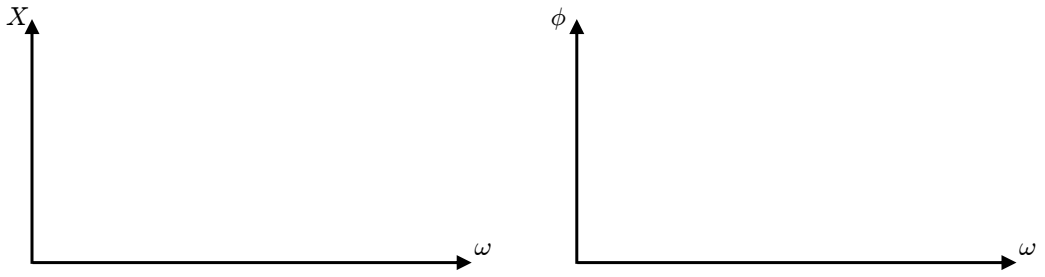

Chapter 18

Pressure Sensors

18.1 Overview

Research related to micromachined pressure sensors is quite mature. This largely stems from the fact that the application area predates the MEMS/NEMS revolution. Additional information related to these systems can be found in [10], from which most of this module was adapted.

Modern, small-scale pressure sensors typically consist of a suspended plate or membrane whose motion is sensed piezoresistively or capactively.

In general, there are three types of MEMS pressure sensors:

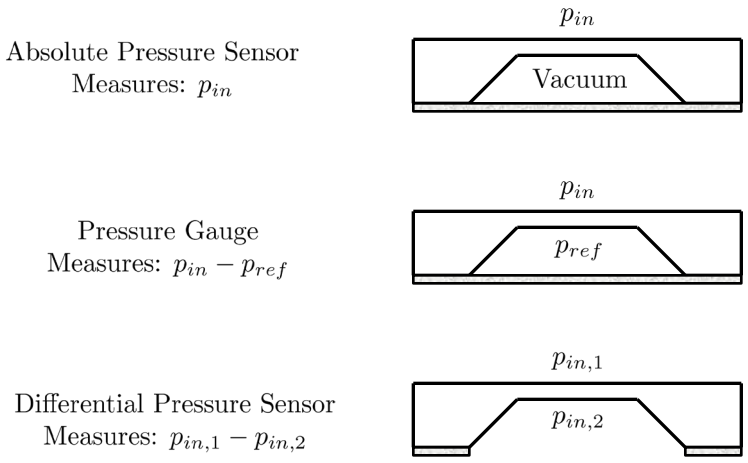

While these sensors come in a variety of shapes and sizes, square and circular designs dominate the market.

18.2 Circular Pressure Sensors

Recall that the dynamics of a circular plate in bending are governed by:

$$D\nabla^4 w(r,\theta,t) + \rho h \frac{\partial^2 w(r,\theta,t)}{\partial t^2} = f(r,\theta,t), \tag{18.1}$$

where

$$D = \frac{Eh^3}{12(1-\nu^2)} \tag{18.2}$$

is the flexural rigidity of the plate, ρ, E and ν are the mass density, modulus of elasticity and Poisson's ratio associated with the plate, h represents the plate's thickness, and $f(r,\theta,t)$ is the applied force per unit area or pressure to be measured.

Ignoring angular variations and assuming quasistatic behavior yields:

(18.3)

where p is the applied pressure.

This equation can be integrated to obtain $w(r)$ in terms of a series of unknown constants c_i:

(18.4)

Since $w(r)$ must be bounded $c_2 = c_3 = 0$. Enforcing this yields:

(18.5)

Applying a clamped boundary condition yields:

(18.6)

(18.7)

Substituting appropriately:

(18.8)

Accordingly:

(18.9)

The deflection at the center of the plate is often an important design quantity:

(18.10)

Likewise, if is often important to know the stresses induced by plate bending, which can be calculated using classical techniques:

(18.11)

(18.12)

These equations reveal that the maximum stress occurs at the plate's boundary where $r = R$, the radius of the plate:

(18.13)

(18.14)

This is the point at which failure is most likely to occur.

At the center, $r = 0$:

(18.15)

18.3 Square Pressure Sensors

By adopting a similar solution approach to that utilized above, it can be shown that the behavior of a square pressure sensor with edge length $2a$ is governed by:

(18.16)

(18.17)

(18.18)

(18.19)

As with the circular configuration, boundary stresses tend to be the highest in square pressure sensors and stresses at or near the center are appreciably smaller.

18.4 Transduction Mechanisms

The above section detail the relationships between the applied pressure p and resulting deflection w, to utilize this within the context of MEMS the deflection w must also be related to a measurable

quantity. This relationship, of course, depends on the transduction method which is selected.

If piezoresistive sensing is selected, the change in resistance ΔR is measured. Recall,

(18.20)

where R is the nominal resistance of the system, π_l and π_t are piezoresistive coefficient and σ_l and σ_t are induced stresses in the longitudinal and transverse directions respectively.

If capacitive/electrostatic sensing is utilized, the changes in capacitance C are measured. Recall,

(18.21)

where A is the electrode area, ε is the permittivity of the gap medium, and g is the nominal gap width.

Example 18.1

Given: Consider a 1 mm $\times$ 1 mm square pressure sensor that is 10 μm thick. The sensor is made of single-crystal silicon ($E = 70$ GPa and $\nu = 0.06$). Assume the sensor can be modeled as a square plate which is clamped on the boundaries.

Find:

(a) Find an input/output relationship between the applied pressure p and resistance change ΔR, if piezoresistive elements are located on the $x = \pm a$ boundaries where $y = 0$. Assume $\pi_l = 70 \times 10^{-11}$ /Pa and $\pi_t = -66 \times 10^{-11}$ /Pa.

(b) Find an input/output relationship between the applied pressure p and capacitance change ΔC, if the nominal gap between plate and grounded substrate is $g = 3$ μm.

Chapter 19

Non-resonant Mass Sensors

19.1 Overview

Another class of MEMS/NEMS which utilize quasistatic behaviors for practical gain and have received considerable research attention over the past two decades is non-resonant mass sensors. These devices utilize the measured deflection of a micro/nanostructure to signal the presence of a target analyte.

The prototypical example of a non-resonant mass sensor is a functionalized microcantilever.

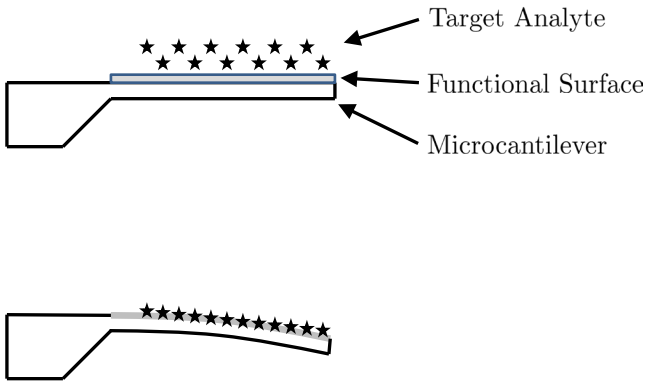

The displacement of these systems is typically measured optically or with a piezoresistive element.

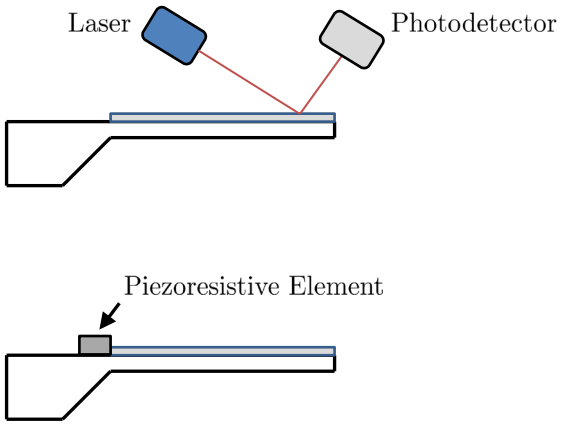

19.2 Sensor Deflection

The deflection in non-resonant mass sensors is induced by the fact that as analytes adsorb or absorb onto/into the sensors' functionalized surface a change in mass, stiffness, and/or surface stress results.

The adsorbate-induced deflections of thin plates (or beams) are governed by Stoney's Formula [21]:

(19.1)

Here, ρ is the radius of curvature of the structure, ν is Poisson's ratio, E is the modulus of elasticity associated with the device, t is the thickness of the structure, and $\Delta\sigma$ is the chemomechanically-induced change in surface stress. Please note that this equation assumes that there is negligible mechanical contributions from the functional layer.

Using techniques introduced in previous modules, the radius of curvature can be related to the tip deflection of the structure yielding:

(19.2)

where L is the length of the structure. By measuring this tip deflection directly or the curvature of the structure indirectly (i.e. via a piezoresistive element) the presence of a target analyte can be detected.

19.3 Calormetric Sensing

Apart from induced surface stresses, calormetric-based sensing can also be used for analyte detection. The idea here is to either (i) detect the presence of target analytes through the detection of heat associated with the adsorption process; or (ii) detect the heat associated with a chemical reaction induced on the surface of the sensor. To realize this approach, a bi-metallic or bimorph structure is typically utilized.

Recall,

$$\frac{1}{\rho} = \frac{6w_1w_2E_1E_2t_1t_2\left(t_1+t_2\right)\left(\alpha_1-\alpha_2\right)\Delta T}{\left(w_1E_1t_1\right)^2+\left(w_2E_2t_2\right)^2+2w_1w_2E_1E_2t_1t_2\left(2t_1^2+3t_1t_2+2t_2^2\right)}, \tag{19.3}$$

where E_1, E_2, α_1, and α_2 represent the modulus of elasticity and thermal expansion coefficient of each bimorph layer, respectively, w_1, w_2, t_1 and t_2 represent the width and thickness of each bimorph later, respectively, and ΔT is the associated temperature change.

The tip deflection associated with this system can be expressed as:

$$\Delta z \approx \frac{L^2}{2\rho} \tag{19.4}$$

where L is the length of the structure.

These equations can be used to detect a change in temperature ΔT, or, assuming here $w_1 = w_2$, be used to measure and absorbed power P:

(19.5)

where

(19.6)

and λ_1 and λ_2 are the thermal conductivity of each layer. This approach can be used to measure sub-fJ units of energy.

Example 19.1

Given: It has been reported that the induced surface stress due to biomolecular interactions are on the order of $\Delta\sigma = 3 \times 10^{-3}$ N/m. Gold coated, silicon cantilevers measuring 500 μm $\times$ 100 μm $\times$ 1 μm are used for detection.

Find: The tip deflection induced by the biomolecular interaction.

Chapter 20

Accelerometers

20.1 Overview

Accelerometers are arguably some of the most pervasive MEMS/NEMS devices, as they appear in applications ranging from automobile safety and laboratory diagnostics to personal gaming.

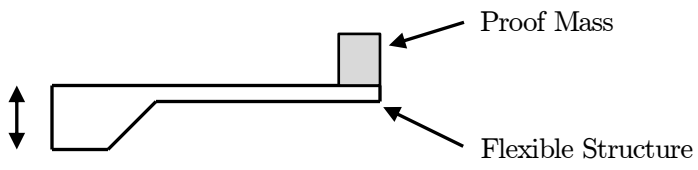

In general, accelerometers consist of a proof mass anchored via flexures to a movable frame. This is often exemplified by a system akin to that shown below.

Though prior modules have provided the necessary tools to develop distributed-parameter models for accelerometers, most of these yield an identical lumped-mass model, so this simplified representation is the focus of the present chapter.

20.2 Lumped-Mass Accelerometer Model

Uniaxial accelerometers are typically modeled as single-degree-of-freedom spring mass systems (see below). Three-axis analogs are often built in practice, but in most cases these are comprised of three uniaxial systems.

The displacement of the moving mass within an accelerometer is typically measured via piezoresistive, piezoelectric, or capacitive means. Of these, capacitive devices are the most common, due to their superior noise characteristics, power consumption metrics, and low-frequency measurement capability.

The equation of motion for a uniaxial accelerometer can be recovered by applying Newton's Second Law to the system shown above:

(20.1)

Here, m, c, and k represent the system's effective mass, damping, and stiffness, x is the absolute displacement of the accelerometer, and x_b is an imposed base motion.

It proves convenient to introduce a relative coordinate z:

(20.2)

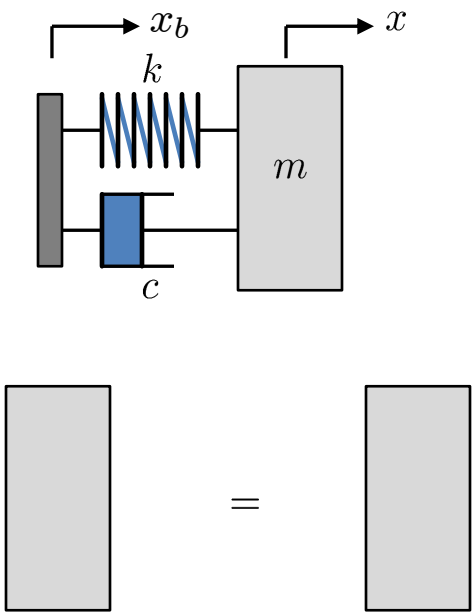

Substituting yields:

(20.3)

which is often written as:

(20.4)

Scaling this result yields:

(20.5)

Which can be rewritten as:

(20.6)

where Q and ω_n are the quality factor and natural frequency associated with the system respectively. Assuming $x_b = b \sin \omega t$, and using results from previous modules, this can be expressed as:

(20.7)

Note:

- If $\omega << \omega_n$ (i.e. there is a low-frequency response), then:

(20.8)

  Note that typical natural frequency for low-frequency systems range from 10 Hz to 10 kHz. These low frequencies are commonly obtained through the use of creative geometries or large proof masses.

- If $\omega >> \omega_n$ (i.e. there is high-frequency response), then:

(20.9)

  That is, the proof mass essentially doesn't move with respect to the moving frame. This type of sensor is extremely difficult to implement at small scales, as it is roughly the equivalent of attempting to build a small-scale seismometer.

Though the above characterized displacement behaviors are important in accelerometer design, the dynamic nature of an accelerometer's response is also pertinent.

Recall the results summarized below:

- If $Q > 0.5$ the system is *underdamped*.
- If $Q = 0.5$ the system is *critically damped*.
- If $Q < 0.5$ the system is *overdamped*.

An accelerometer's displacement error is defined to be:

(20.10)

where τ is a characteristic time constant. Note that:

- If $Q > 0.5$, $\tau \approx \frac{2Q}{\omega_n}$.
- If $Q < 0.3$, $\tau \approx \frac{1}{Q\omega_n}$.
- If $0.3 < Q < 0.5$, then the time constant should be determined via simulation.

Note that $Q = 0.5$ is often optimal for MEMS accelerometers.

20.3 The Impact of Thermomechanical Noise

The ultimate performance of accelerometers is often bounded by thermal noise:

(20.11)

where $\bar{\ddot{x}_n}$ is the spectral density of acceleration, $\bar{F_n}$ is the spectral density of the equivalent noise force, k_B is Boltzman's constant, and T is the temperature of the system.

Alternatively, recall:

(20.12)

The takeaway from this result is that Q has no effect on the net noise, but increasing m and/or lowering ω_n can help mitigate its effects.

Example 20.1

Given: Consider a silicon accelerometer ($\rho = 2330$ kg/m^3) with a proof mass measuring 1200 μm $\times$ 1200 μm $\times$ 550 μm. The accelerometer has a net stiffness of $k = 40$ N/m and an associated quality factor of $Q = 0.2$.

Find:
(a) The natural frequency of the system ω_n;
(b) The damping constant associated with the system c;
(c) The magnitude of displacement $|z|$ under a 1-g load at low frequencies;
(d) The spectral density of displacement $\bar{x_n}$ at room temperature due to thermal noise;
(e) The rms response x_{rms} due to thermal noise; and
(f) The spectral density of acceleration $\bar{\ddot{x}_n}$ due to thermal noise.

Chapter 21

Radio-Frequency (RF) Switches

21.1 Overview

Radio-frequency (RF) switching is a rapidly emerging market, spurned by the growth in global telecommunications. Currently, two types of switches dominate the market:

- *Mechanical Switches and Relays*, which are highly reliable, but bulky and expensive; and
- *Solid-State Switches and Relays*, which are comparatively small and cheap, but feature poor power consumption, linearity, and signal loss metrics.

RF MEMS/NEMS switches seek to take advantage of their unique electromechanical nature to offer the best of both worlds. Unfortunately, they feature their own lists of pros and cons:

- The Good:
  - Comparatively linear response;
  - Minimal parasitic capacitance;
  - Low insertion loss;
  - Comparatively cheap; and
  - Low power consumption.
- The Bad:
  - Switching speed
- The Ugly:
  - Poor reliability

To date, the vast majority of micro/nanosale switches have exploited Ohmic contact or changes in capacitance. This module considers each switch type in turn by building upon the work of [10].

21.2 Capacitive Switches

Capacitive switches exploit large, abrupt changes in capacitance for switching, as shown below.

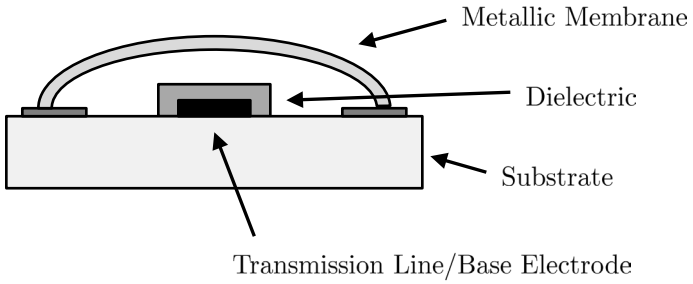

When the membrane is in the *up* state, there is a small capacitance to ground, and thus the signal passes with minimal attenuation.

In contrast, when the membrane is in the *down* state, there is a large capacitance to ground, which leads to an effective grounding of the signal.

The performance of a capacitive switch is typically expressed in terms of a power ratio S_{21}:

(21.1)

where V_{in} and V_{out} are the voltages coming into and leaving the switch respectively, ω is the signal frequency, C is the bridge capacitance, and Z_0 is the transmission line impedance.

Actuation in this system is achieved via electrostatic pull-in. Typically, the static pull-in voltage is computed, and voltages in excess of this are used for actuation. Recall that for a lumped-mass model:

$$V_{PI} = \sqrt{\frac{8kg_0^3}{27\varepsilon A}} \tag{21.2}$$

where k is the effective stiffness of the system, ε is the permittivity of the gap medium, g_0 is the nominal gap width, and A is the effective electrode area.

After a switch is activated, less voltage is required to hold it in position. For example, suppose a switch deflection Δx is achieved after actuation. In a static sense, this means that the elastic restoring force is balanced by the electrostatic force. This implies that:

(21.3)

where ε_r and ε_0 are the relative and absolute permittivities of the gap medium, g is the effective gap width, and V_{DC} is the applied DC actuation voltage. Solving this expression for V_{DC} yields:

(21.4)

If an AC voltage V_{AC} is used in place of a DC voltage, the holding voltage can be estimated by:

(21.5)

Please note that all of these voltages are conservative estimates. In addition, these equations reveal a key concern with capacitive switches, namely due to the presence of a voltage difference near the contact point dielectric charging and stiction are possible. This fact has hindered the broad implementation of capacitive switches.

21.3 Ohmic Switches

Ohmic switches (shown below), much like their capacitive counterparts, leverage pull-in for actuation purposes. However, Ohmic switches offer appreciably larger off/on capacitance ratios, which makes them rather appealing from a signal processing point of view. Unfortunately, this benefit comes hand-in-hand with a series of robustness issues associated with contact resistance and contact force/deformation.

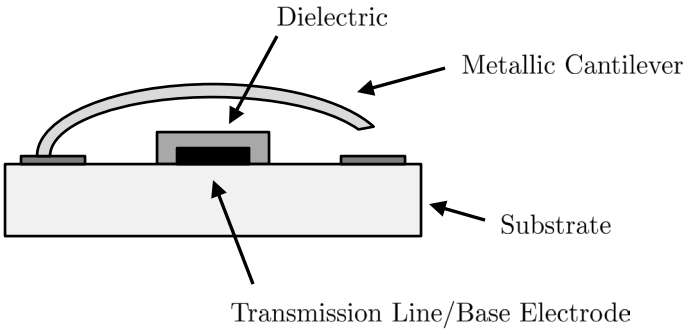

21.4 Switching Speeds

As previously noted in the module, MEMS/NEMS switches are commonly limited by switching speeds. In general, optimal switching speeds in these systems can be realized by operating with quality factors Q near $0.2 < Q < 0.5$. Though accurate estimates of switching time are difficult to produce, a few approximations have been proposed.

If $Q > 1$, and the switching voltage $V_s > 1.3V_{PI}$, then the closing speed t of a MEMS/NEMS switch can be estimated as:

(21.6)

where ω_n is the natural frequency of the system. Generally speaking, this relationship estimates experimental values within 10%.

If $0.1 < Q < 1$, and the switching voltage $V_s > 1.15V_{PI}$, then the closing speed t can be estimated as:

(21.7)

where

(21.8)

(21.9)

Generally speaking, this relationship estimates experimental values within 20%.

The opening speed of a switch, which contributes to the switch's total duty cycle, can be estimated by:

(21.10)

Generally speaking, this relationship estimates experimental values within 20%.

Chapter 22

Resonant Mass Sensors

22.1 Overview

Previously in this lecturebook, the behavior of mass sensors which utilize static/quasistatic bending to signal the presence of a target analyte were considered. The present module considers a variation of this sensor which exploits changes in resonant behavior to signal the presence of the aforementioned analytes.

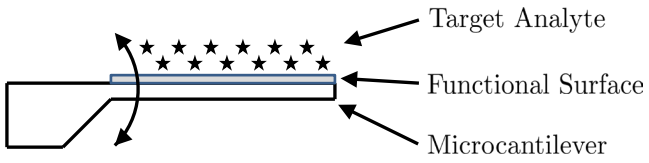

The operating principle upon which resonant mass sensors are founded is quite simple: Changes in the mass or stiffness of a system lead to changes in the system's natural frequency. If this change in natural frequency can be identified, or better yet quantified, then sensing can be realized. In fact, this technique has proven itself to be very fruitful in experimentation, as it has facilitated the detection of sub-zeptogram masses ($< 10^{-21}$ g of substance).

Generally speaking resonant mass sensors are transduced through a local piezoelectric element, via electrostatic means, or using a piezo-stack actuator.

22.2 Sensor Modeling

Though distributed-parameter representations of resonant mass sensors can be easily developed, most yield a lumped-parameter model akin to:

(22.1)

where m, c, and k are the effective mass, damping, and stiffness associated with the system, x is a local displacement variable, and $F(t)$ is an applied actuation force. It is important to note that m, c, and k will change in the presence of a target analyte. To ensure that added-mass effect dominate, resonant sensors are typically functionalized near their tips.

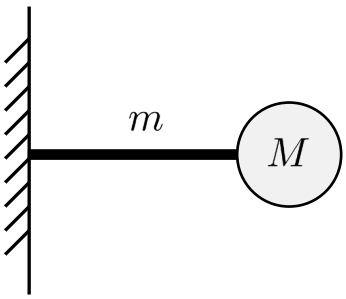

Assuming operation near the first mode:

(22.2)

For a cantilever:

(22.3)

where E is the elastic modulus associated with the system, and b, t, and L represent the beam's width, thickness, and length. Accordingly,

(22.4)

Though this equation is commonly used in design and experimental interpretation, it is important to remember that the maximum amplitude of vibration does not occur at the natural frequency ω_n in the presence of damping.

22.3 Performance Metrics

Though, in practice, it would be nice to immediately attribute changes in frequency to an added-mass effect, slightly more care must be taken.

To first order, assuming tip mass addition:

(22.5)

where ω_0 is the natural frequency of the system with tip mass M and ω_1 is the natural frequency of the system with tip mass $M + \Delta M$.

Generalizing this result, the *mass responsivity* of the sensor S_m can be recovered:

(22.6)

where $\Delta\Gamma = \Delta M/A$ and A is the active sensor area.

Again assuming a microcantilever with added tip mass:

(22.7)

where ρ is the mass density of the beam and t is the beam's thickness. To compute the sensor's *minimal detectable mass* $\Delta\Gamma_{min}$ one can use:

(22.8)

Here, $\Delta\omega_{min}$ is the smallest change in frequency which can be resolved in the presence of noise. In theory, this quantity is limited by the thermal noise contribution (k_BT). However, in practice, only a fraction of a Hz change in natural frequency can be detected repeatably.

Chapter 23

Radio-Frequency (RF) Signal Filters

23.1 Overview

Since the earliest dates of the MEMS/NEMS community, frequency-selective filters have been a cornerstone of the field. These devices have been built on a number of technology platforms (e.g. bulk acoustic wave, contour-mode, planar silicon, microcantilevers, etc.), have utilized a wide variety of transduction mechanisms, and have been comprised of isolated or coupled micro/nanoresonators. Despite a clear demand for a variety of filter types, research and development effort have largely focused on bandpass filters, which is the principal focus of this module.

An ideal bandpass filter exhibits the *box car* frequency response characteristic shown below.

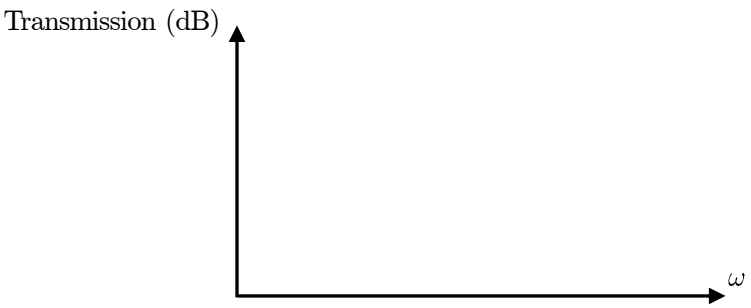

Unfortunately, this response characteristic is difficult to recover in practice, leading to the following alternative. Note that in both of these figures, transmission is defined to be:

(23.1)

where A is the output signal amplitude and A_{max} is the peak, in-band response amplitude.

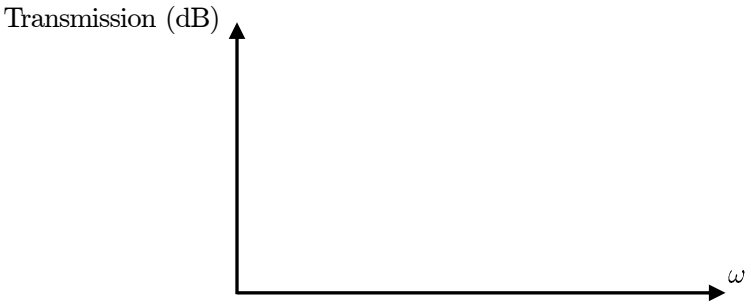

23.2 Performance Metrics

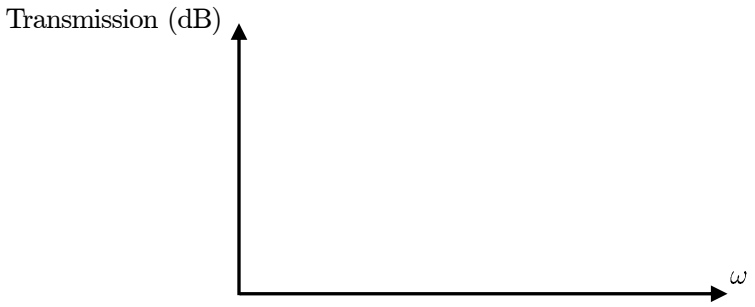

The performance of bandpass filters is commonly characterized via the following metrics:

- The *cut-off frequencies*, ω_{c1} and ω_{c2} are defined from the half-power points of the spectrum or at 3 dB attenuation.
- The *bandwidth*, $BW = \omega_{c2} - \omega_{c1}$ is defined to be the width of the filter passband.
- The *center frequency*, $CF = (\omega_{c1} + \omega_{c2})/2$, is defined to be the average value of the cut-off frequencies.
- The *effective quality factor* associated with the system is defined to be $Q_{eff} = CF/B$.
- The *N dB shape factor* associated with the system is defined to be the ratio of the N dB bandwidth and 3 dB bandwidth.
- The *ripple* is defined to be the difference between the minimum and maximum in-band response.
- The *insertion loss* is defined to be the ratio of the signal level without the filter installed to the signal level with the filter installed (in dB).
- The *roll-off* is the rate of transition between the stopband and passband.

Generally speaking, for RF applications, the following characteristics are desirable:

- High center frequency (2 MHz - 300 GHz)
- Low bandwidth ($Q_{eff} > 5000$).
- Low insertion loss
- Low ripple

23.3 The Simple Solution: A Single Resonator Solution

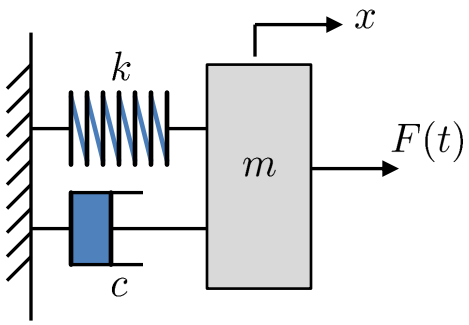

The simplest electromechanical bandpass filter that can be implemented is a single-degree-of-freedom (SDOF) resonator, akin to that shown below. As previously demonstrated, the equation of motion governing this system can be written as:

(23.2)

where m, c, and k are the system's effective mass, damping, and stiffness, x is a local displacement variable, and $F(t)$ is an applied actuation force. This can be rewritten in terms of the system's natural frequency ω_n and quality factor Q as:

(23.3)

The transmission characteristic associated with this (SDOF) is shown below.

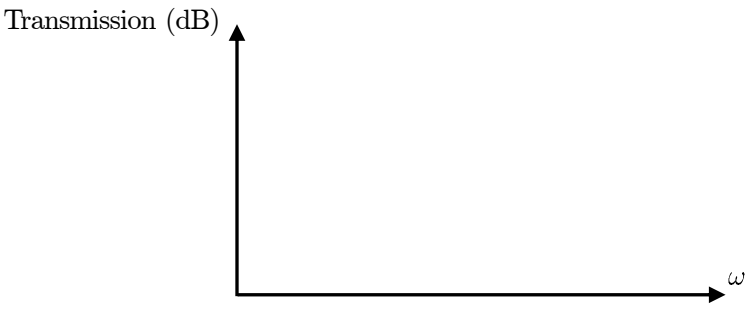

The center frequency associated with this filter is given by

(23.4)

if $Q > \sqrt{2}/2$. If Q is very large, then $CF \approx \omega_n$.

The effective quality factor associated with the system $Q_{eff} = Q$.

Generally speaking, filters based on SDOF resonator have high center frequencies, high effective quality factors, and low insertion loss. Unfortunately, they suffer with respect to other metrics. One cleaver way to circumvent this constraint is to coupled multiple resonators together, creating in essence a MEMS/NEMS ladder filter.

23.4 Filters Based on Coupled Microresonators

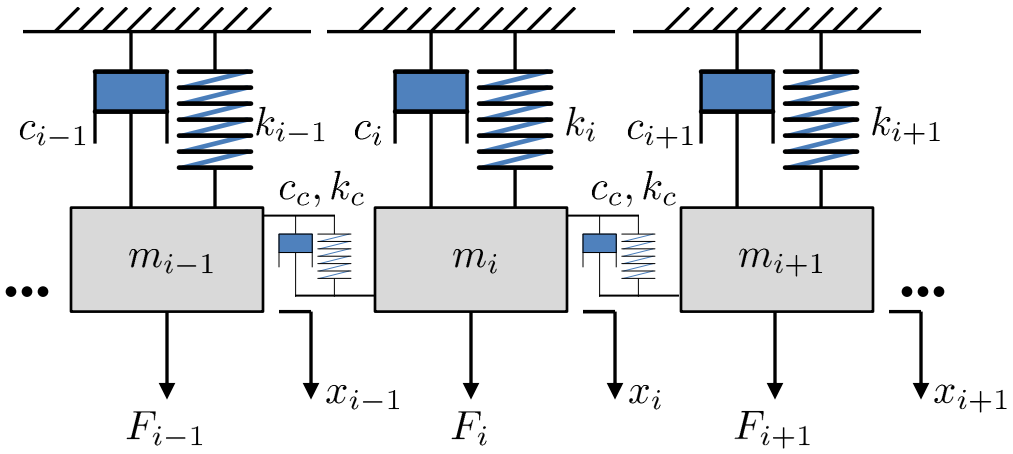

Consider a multi-degree-of-freedom resonator system akin to that considered in previous chapters. Applying Newton's Second Law to the ith element of this system yields:

(23.5)

where all parameters are defined as in the diagram. This can be rewritten in matrix form as:

(23.6)

where, assuming all elements are equal,

(23.7)

(23.8)

(23.9)

(23.10)

(23.11)

This system of equations can be solved by utilized the previously-introduced impedance approach. To realize this, first assume the excitation and response are time harmonic:

(23.12)

(23.13)

Substituting yields:

(23.14)

This can be re-written as:

(23.15)

where the complex impedance matrix $\mathbf{Z}$ is defined as

(23.16)

Inverting the result renders:

(23.17)

which can be analyzed to recover the amplitude and phase response of the system.

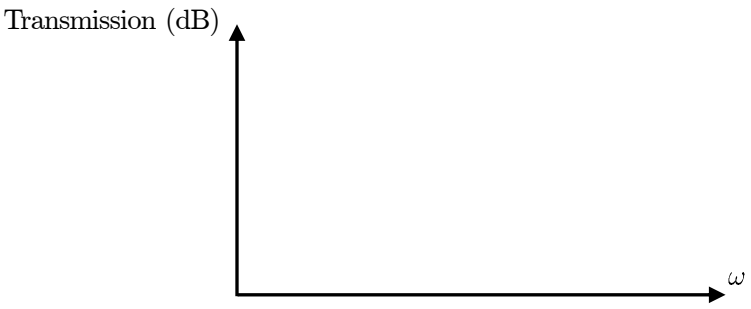

Generally speaking, the exploitation of coupled microresonators in filtering applications leads to a decrease in the effective quality factor and an increase in insertion loss, yet an improvement to most other metrics. This statement, however, depends on wise selection of the coupling stiffness k_c and the damping constant associated with the system c.

Finally, note that the analysis included herein focused on identical substructures. If some mistuning in frequency exists within the system, the recovered response may be markedly more complex than predicted to the existence of Anderson Localization.

Appendix A

References

[1] R. P. Feynman, "There's plenty of room at the bottom (reprint)," *Journal of Microelectromechanical Systems*, vol. 1, no. 1, pp. 60–66, 1992.

[2] R. P. Feynman, "Infinitesimal machinery (reprint)," *Journal of Microelectromechanical Systems*, vol. 2, no. 1, pp. 4–14, 1993.

[3] H. C. Nathanson and R. A. Wickstrom, "A resonant-gate silicon surface transistor with high-q band-pass properties," *Applied Physics Letters*, vol. 7, no. 4, pp. 84–86, 1965.

[4] H. C. Nathanson, W. E. Newell, R. A. Wickstrom, and J. R. Davis Jr., "The resonant gate transistor," *IEEE Transactions on Electron Devices*, vol. 14, no. 3, pp. 117–133, 1967.

[5] K. Petersen, "Silicon as a mechanical material," *Proceedings of the IEEE*, vol. 70, no. 5, pp. 420–457, 1982.

[6] A. N. Cleland, *Foundations of Nanomechanics: From Solid-State Theory to Device Applications*. Advanced Texts in Physics, Berlin: Springer, 2003.

[7] C. Liu, *Foundations of MEMS*. Illinois ECE Series, Upper Saddle River, New Jersey: Pearson/Prentice Hall, 2006.

[8] J. A. Pelesko and D. H. Bernstein, *Modeling MEMS and NEMS*. Boca Raton, Florida: Chapman & Hall/CRC, 2002.

[9] M. I. Younis, *MEMS Linear and Nonlinear Statics and Dynamics*. Microsystems, New York, New York: Springer, 2011.

[10] V. Kaajakari, *Practical MEMS*. Las Vegas, Nevada: Small Gear Publishing, 2009.

[11] S. S. Rao, *Vibration of Continuous Systems*. Hoboken, New Jersey: John Wiley and Sons, Inc., 2007.

[12] L. R. Calcote, *The Analysis of Laminated Composite Structures*. New York, New York: Van Nostrand Reinhold Company, 1969.

[13] V. Kumar, J. W. Boley, Y. Yang, H. Ekowaluyo, J. K. Miller, G. T.-C. Chiu, and J. F. Rhoads, "Bifurcation-based mass sensing using piezoelectrically-actuated microcantilevers," *Applied Physics Letters*, vol. 98, p. 153510, 2011.

[14] H. B. Chan, V. A. Aksyuk, R. N. Kleiman, D. J. Bishop, and F. Capasso, "Quantum mechanical actuation of microelectromechanical systems by the casimir force," *Science*, vol. 291, no. 5510, pp. 1941–1944, 2001.

[15] J. E. Sader, "Frequency response of cantilever beams immersed in viscous fluids with applications to the atomic force microscope," *Journal of Applied Physics*, vol. 84, no. 1, pp. 64–76, 1998.

[16] M. J. Martin and B. H. Houston, "Computation of damping for vibrating micro-machined cantilevers in the slip flow regime," January 7-10, 2008 2008.

[17] F. R. Blom, S. Bouwstra, M. Elwenspoek, and J. H. J. Fluitman, "Dependence of the quality factor of micromachined silicon beam resonators on pressure and geometry," *Journal of Vacuum Science and Technology B*, vol. 10, no. 1, pp. 19–26, 1992.

[18] R. A. Bidkar, R. C. Tung, A. A. Alexeenko, H. Sumali, and A. Raman, "Unified theory of gas damping of flexible microcantilevers at low ambient pressures," *Applied Physics Letters*, vol. 94, no. 16, p. 163117, 2009.

[19] V. T. Srikar and S. D. Senturia, "Thermoelastic damping in fine-grained polysilicon flexural beam resonators," *Journal of Microelectromechanical Systems*, vol. 11, no. 5, pp. 499–504, 2002.

[20] V. B. Braginsky, V. P. Mitrofanov, and V. I. Panov, *Systems with Small Dissipation*. Chicago: The University of Chicago Press, 1985.

[21] N. V. Lavrik, M. J. Sepaniak, and P. G. Datskos, "Cantilever transducers as a platform for chemical and biological sensors," *Review of Scientific Instruments*, vol. 75, no. 7, pp. 2229–2253, 2004.